Liver Receptor Homolog-1 Regulates Kisspeptin Expression in the Arcuate Nucleus to Promote Reproductive Axis Function

APPROVED BY SUPERVISORY COMMITTEE

David Mangelsdorf, Ph.D.
Steven Kliewer, Ph.D.
Joel Elmquist, DVM, Ph.D.
Joseph Takahashi, Ph.D.
Carole Mendelson, Ph.D.

To

My wife, Lindsee, and my parents Thomas & Jane

LIVER RECEPTOR HOMOLOG-1 REGULATES KISSPEPTIN EXPRESSION IN THE ARCUATE NUCLEUS TO PROMOTE REPRODUCTIVE AXIS FUNCTION

by

STAN DEAN ATKIN

DISSERTATION

Presented to the Faculty of the Graduate School of Biomedical Sciences

The University of Texas Southwestern Medical Center at Dallas

In Partial Fulfillment of the Requirements

For the Degree of

DOCTOR OF PHILOSOPHY

The University of Texas Southwestern Medical Center at Dallas

Dallas, Texas

June, 2012

ACKNOWLEDGEMENTS

I would like to thank David Mangelsdorf and Steven Kliewer for their support and mentorship during my time in their lab. They work tirelessly to create an environment of readiness and virtuosity that might prepare us for whatever nature brings our way. It goes without saying that I couldn't have done any of this without the present and past lab members, whose thoughts, guidance, and selfless dedication to science helped me more than I can appreciate. I thank my committee, as well, for their expertise and interest in seeing to the growth of my career and development as a scientist.

I would especially like to thank my wife, Lindsee Atkin, for being the most influential and inspiring person I know. I couldn't do any of this without her. I know there were some days in there where she even put my socks on for me. She is a beautiful grain of salt amongst at times a barren and tasteless world, and while I know this world could use more like her, I'm glad she's all mine. Of course, my children, for bringing new laughter and beauty into my life with every smile.

Lastly, I want to thank Dr. Janine Trempy at Oregon State University. She recognized the fight in me when I only recognized the free spirit. I can't thank her enough for picking me up by my heel, brushing me off, and making a doctor out of me.

LIVER RECEPTOR HOMOLOG-1 REGULATES KISSPEPTIN EXPRESSION IN THE ARCUATE NUCLEUS TO PROMOTE REPRODUCTIVE AXIS FUNCTION

STAN DEAN ATKIN, Ph.D.

The University of Texas Southwestern Medical Center at Dallas, June 2012

DAVID J. MANGELSDORF, Ph.D. & STEVEN A. KLIEWER, Ph.D.

The timing of ovulation in mammals is set by a complex hypothalamic pituitary neuroendocrine axis. Kisspeptin neurons in the arcuate nucleus (Arc) are thought to secrete kisspeptin (Kiss1) to stimulate the release of follicle stimulating hormone (FSH) from the pituitary. However, mechanisms that drive Arc KISS1 output and maintain adequate FSH secretion required for folliculogenesis are not

well understood. Here, we report that the nuclear receptor, liver receptor homolog-1 (LRH-1), is expressed in kisspeptin neurons of the Arc. *Kiss1* is found to be a direct target gene of LRH-1, whereby LRH-1 sets a basal tone of *kiss1* expression in the Arc. Deletion of *Lrh-1* from kisspeptin neurons causes decreased Arc *Kiss1* expression. This leads to reduced plasma FSH, prolongation of the estrous cycle, and decreased follicle maturation and ovulation. These defects ultimately compromise fertility. Overexpression of *Lrh-1* in a kisspeptin neuron-specific transgenic mouse model increases Arc *Kiss1* expression and plasma FSH. Chromatin immunoprecipitation and luciferase-based promoter assays demonstrate that LRH-1 binds to a putative LRH-1 response element in the *Kiss1* promoter to stimulate activity. In conclusion, LRH-1 is expressed in the Arc to set the basal tone of *Kiss1* output needed to promote FSH secretion for folliculogenesis prior to ovulation.

TABLE OF CONTENTS

Chapter One

Liver Receptor Homolog-1 and the Hypothalamic Control of Energy Status and Reproduction

Chapter Four

Kiss1 is an LRH-1 *Target Gene*

Chapter Five

The Role of LRH-1in POMC Neurons

Chapter Six

Closing Remarks and Future Directions

Chapter Seven

Materials & Methods

PRIOR PUBLICATIONS

Atkin SD, Patel S, Kocharyan A, Holtzclaw LA, Weerth SH, Schram V, Pickel J, Russell JT. Transgenic mice expressing a cameleon fluorescent Ca2+ indicator in astrocytes and Schwann cells allow study of glial cell Ca2+ signals in situ and in vivo. J Neurosci Methods. 2009 Jul 30;181(2):212-26. Epub 2009 May 18.

Besser L, Chorin E, Sekler I, Silverman WF, **Atkin S**, Russell JT, Hershfinkel M. Synaptically released zinc triggers metabotropic signaling via a zinc-sensing receptor in the hippocampus. J Neurosci. 2009 Mar 4;29(9):2890-901.

Cravo RM, Margatho LO, Osborne-Lawrence S, Donato J Jr, **Atkin S**, Bookout AL, Rovinsky S, Frazão R, Lee CE, Gautron L, Zigman JM, Elias CF. Characterization of Kiss1 neurons using transgenic mouse models. Neuroscience. 2011 Jan 26;173:37-56. Epub 2010 Nov 18.

Sephton CF, Good SK, **Atkin S**, Dewey CM, Mayer P 3rd, Herz J, Yu G. TDP-43 is a developmentally regulated protein essential for early embryonic development. J Biol Chem. 2010 Feb 26;285(9):6826-34. Epub 2009 Dec 29. Erratum in: J Biol Chem. 2010 Dec 3;285(49):38740.

LIST OF FIGURES

LIST OF ABBREVIATIONS

Arc	Arcuate nucleus of the hypothalamus
AF-1	Activation function-1
AF-2	Activation function-2
AVPV	Anteroventral periventricular nucleus of the hypothalamus
ChIP	Chromatin Immunoprecipitation
Cyp#x#	Cytochrome P450 (number)(letter)(number); i.e. Cyp P450 7a1.
DAX-1	Dosage sensitive sex reversal, adrenal hypoplasia critical region on chromosome x gene 1
DBD	DNA binding domain
DNA	Deoxyribonucleic acid
E2	Estradiol
ERα	Estrogen receptor alpha
FACS	Fluorescence assisted cell sorting
FSH	Follicle stimulating hormone
FTZ-F1	Fushi-tarazu-F1
FXR	Farnesoid X Receptor
GFP	Green fluorescent protein
GnRH	Gonadotropin releasing hormone
GnRHr	Gonadotropin releasing hormone receptor
GPR54	G-protein coupled receptor 54
HFD	High fat diet
IgG	Immunoglobulin G
ISH	In situ hybridization
KISS1	Kisspeptin
KO	Kiss1 specific Lrh-1 knockout mouse
LBD	Ligand binding domain
LH	Luteinizing Hormone

LRH-1	Liver receptor homolog-1
LRHRE	Lrh-1 response element
Lrh-Tg	Kiss1 specific Lrh-1 Transgenic mouse
LXR	Liver X receptor
Luc	Luciferase
MRI	Magnetic resonance imaging
mRNA	Messenger-ribonucleic acid
NPY/AgRP	Neuropeptide Y/agouti-related peptide
NRE	Nuclear response element
OCT-4	Octamer binding transcription factor-4
pKO	Pomc specific Lrh-1 knockout mouse
Pomc	Pro-opiomelanocortin/α-melanocyte stimulating hormone
QPCR	Quantitative reverse transcriptase polymerase chain reaction
RXR	Retinoid X Receptor
SCN	Suprachiasmatic nucleus
SF-1	Steroidogenic factor-1
SHP	Small heterodimer
StAR	Steroid acute regulatory enzyme
TdT-KO	Tomato-lox/stop/lox Lrh-1 knockout mouse
THR	Tyrosine hydroxylase
WT	Wildtype mice

CHAPTER ONE

Liver Receptor Homolog-1 and the Hypothalamic Control of Energy Status and Reproduction

1.1 Overview

Eukaryotic cells have the ability to coordinate and support each other's actions via hormonal communication. Such coordination make possible systems as complex as the human body. Hormones are small molecules produced by one cell that can act upon other cells. Large families of receptors have arisen that bind to hormones to activate cellular responses. Nuclear hormone receptors are named so because of their localization within the nucleus of eukaryotic cells. They bind hormone ligands and interact with specific regions of a cell's DNA to activate or repress the transcription of target genes needed to elicit a cellular response. There are a total of 48 nuclear hormone receptors in humans and 49 in the mouse, and they are influential throughout the body in a multitude of processes ranging from tissue growth, energy expenditure, reproduction, and nutrient uptake and vitamin utilization (Mangelsdorf and Evans 1995; Makishima, Okamoto et al. 1999; Margolis 2008; McEwan and Nardulli 2009).

Nuclear receptors are classified into subfamilies and groups based on their phylogenetic ontology and sequence homology. The nuclear receptor superfamily nomenclature establishes six subfamilies, and follows the format: nr#letter# (Gao, Wang et al.). For instance, liver receptor homolog-1 is classified as nr5a2 (nuclear

receptor subfamily 5, group a, gene 2). There are three major classes of nuclear hormone receptors, 12 classical nuclear receptors, 25 orphan nuclear receptors, and 11 adopted orphan nuclear receptors (Fig 1.1.1 A) (Mangelsdorf and Evans 1995; Chawla, Repa et al. 2001). Classical nuclear hormone receptors bind to endocrine hormones, such as the estrogen receptor, or the thyroid hormone receptor. All other nuclear receptors are classified as orphan nuclear receptors, as no natural ligand is known for them. When their ligand is discovered, they are re-classified as adopted orphan nuclear receptors. Adopted orphan nuclear receptors often bind diet-derived hormones such as mono-oxygenated cholesterols, bile acids, or fat soluble vitamins (Chawla, Repa et al. 2001).

A

Classical Endocrine	
AR	Androgen
ERα,β	Estrogen
GR	Glucocorticoid
MR	Mineralocorticoid
PR	Progesterone

Adopted Orphan	
CAR	xenobiotics
FXR	bile acids
LXRα,β	oxysterols
PPARα,δ,γ	fatty acids
PXR	xenobiotics
RXRα,β,γ	9-Cis RA, DHA

Orphan	
Coup-TFα,β,γ	?
DAX-1	?
ERRα,β,γ	synthetic steroids
GCNF	?
HNF-4α,γ	fatty acids?
LRH-1	phospholipids?
NGFI-Bα,β,γ	?
PNR	?
RORα,β,γ	fatty acids/sterols
RVRα,β	?
SF-1	phospholipids?
SHP	?
TLX	?
TR2,4	?

B

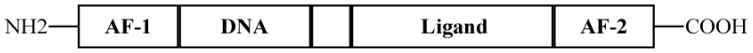

Fig 1.1.1.1 The nuclear receptor super family. A) Categorization of classical and non-classical nuclear receptors by ligand and orphan status. B) Basic subunit structure of nuclear receptors. Activating Helices (AF-1/AF-2) recruit co-activators/co-repressors. DNA binding domain (DNA) contains a zinc finger motif structure. The ligand binding domain (Ligand) is a hydrophobic pocket that binds ligand to initiate target gene transcription.

1.1.2 Nuclear Receptor Structure

The protein structure of almost all nuclear receptors can be divided into four domains (Fig 1.1.1 B). Closest to the N-terminus is the activation function-1 (AF-1) helix. Following this is the DNA binding domain (DBD), the ligand binding domain (LBD), and lastly the activation function-2 (AF-2) helix at the C-terminus of the protein (McEwan and Nardulli 2009). The DBD consists of two zinc-finger structures that bind to the major groove of the DNA helical structure for nuclear receptor-DNA interactions (Helsen, Kerkhofs et al. 2012). DNA

binding occurs at a sequence within the target gene's promoter called a nuclear receptor response elements (NRE). Ligand binding domains are most often large hydrophobic pockets able to bind the cholesterol or lipid derived ligands. The ligand binding domain attaches to the rest of the protein via a hinge region that, upon ligand binding, allows for conformational changes that promote co-activator recruitment. Both the AF-1 and AF-2 helices recruit co-activators and co-repressors to modulate gene transcription (Watson, Fairall et al. 2012). Importantly, the AF-1 helix does this independent of ligand binding, while the AF-2 helix binds co-activators only after ligand binding by the LBD and conformational rearrangement. The AF-2 helix also contains the interface used by nuclear receptors to form homodimers or heterodimers with each other.

NREs have two repeats of a core DNA sequence. This sequences often closely matches a canonical AGGTCA consensus sequence, and the two repeats are usually separated by 1-3 base pairs (Helsen, Kerkhofs et al. 2012). Nuclear receptors dimerize via their AF-2 helices, each monomer binding one of the two NREs and bridging across the interspacing base pairs via AF-2 helix interactions and rotation at the hinge domain. Classical nuclear receptors bind as homodimers, while most orphan nuclear receptors bind as heterodimers with retinoid X receptor (RXR)(Mangelsdorf and Evans 1995). There are a few exceptions to this rule. The nuclear receptors Dax-1 (dosage sensitive sex reversal, adrenal hypoplasia critical region on chromosome x gene 1), and small heterodimer

protein (SHP), do not contain a DBD, and thus do not bind to DNA (Zhang, Thomsen et al. 2000; Denson, Sturm et al. 2001). Instead, they bind directly to the co-activator recruitment locus of the AF-2 helix of other nuclear receptors. This functions to block conventional co-activator recruitment and repress target gene activation by the nuclear receptor. Lastly, a small set of orphan nuclear receptors, LRH-1 and SF-1, do not participate in dimerization, and bind to DNA as monomers. These require only a single response element to activate target gene transcription.

1.2. Liver Receptor Homolog-1

1.2.1 Overview

Liver Receptor Homolog-1 (LRH-1, nr5a2) is an orphan nuclear receptor involved in cholesterol and lipid homeostasis in the liver, and reproductive homeostasis in the ovary and pituitary (Fayard, Auwerx et al. 2004). LRH-1 shares close identity to only one other nuclear receptor, steroidogenic factor-1 (SF-1, nr5a1), and both bind DNA as monomers. Several groups discovered LRH-1 and SF-1 in the early 1990's due to their close homology to the well-characterized zebra fish protein, fushi-tarazu-F1 (FTZ-F1) (Ellinger-Ziegelbauer, Hihi et al. 1994; Kudo and Sutou 1997; Takase, Nakajima et al. 2000). FTZ-F1, LRH-1, and SF-1 have a unique DBD that recognizes the consensus sequence

YCAAGGYCR, where Y is a pyrimidine and R is a purine. No physiological ligand has been discovered for LRH-1. Phosphorylation and sumoylation have been shown to activate or repress LRH-1 activity, respectively (Lee, Choi et al. 2006). Studies have shown that phospholipids may be a putative ligand. Phospholipids can be found within the LBD upon crystallization of LRH-1, and synthetic phospholipid compounds can activate LRH-1 *in vitro* and activate LRH-1 target gene transcription *in vivo* (Whitby, Dixon et al. 2006; Lazarus, Wijayakumara et al. 2012). However, previous studies demonstrated that LRH-1 is constitutively active and can still activate target gene transcription after considerable mutation, or even removal, of the LBD (Sablin, Krylova et al. 2003).

1.2.2 Biological Function

The biological functions of LRH-1 are diverse and vary significantly during the development of the animal. LRH-1 is constitutively active, and thus it functions to stimulate a constant basal set-point of expression of its target genes. In almost all tissues it is expressed in, this constitutive activity of LRH-1 adheres to three conventions. First, LRH-1 commonly binds to gene promoters in close proximity with a classic or orphan nuclear receptor that responds to endocrine or diet derived hormones (Fernandez-Marcos, Auwerx et al. 2011). This allows LRH-1 to stimulate a basal level of transcription of the gene, while the partnering

nuclear receptor activates or represses the gene promoter in a ligand dependent manner.

Second, LRH-1 often stimulates expression of the class of non-DNA binding orphan nuclear receptors (i.e. DAX-1, SHP) that repress target gene expression. These nuclear receptors can bind to and repress LRH-1 activity. This establishes a negative feedback loop (Ortlund, Lee et al. 2005; Sablin, Woods et al. 2008). For instance, in response to high bile acids in the liver, the repressive orphan nuclear receptor SHP binds LRH-1 and its associated NR, the liver X receptor (LXR), to repress target genes needed for bile acid synthesis (Lee, Schmidt et al. 2008; Out, Hageman et al. 2011). Similarly, in response to the luteinizing hormone (LH) surge in the ovary, the repressive nuclear receptor DAX-1 binds to LRH-1 and the associated estrogen receptor α (ERα), to repress LRH-1 target genes needed for estrogen synthesis and follicular maturation (Lalli, Melner et al. 1998; Sandhoff and McLean 1999; Zhang, Thomsen et al. 2000; Hinshelwood, Repa et al. 2003; Liu, Liu et al. 2003).

The third convention of LRH-1 function is how it is often expressed in the tissues of two organs that are interrelated by a common metabolic process. LRH-1 is expressed in both the liver and intestine, where it works in both to coordinate bile acid synthesis and reabsorption (Mataki, Magnier et al. 2007; Lee and Moore 2008). In the reproductive axis LRH-1 is expressed in both the pituitary and

ovary, where it works in both to stimulate expression of genes needed for fertility (Duggavathi, Volle et al. 2008).

Together, these three conventions of LRH-1 activity allow for spatially separate tissues to establish physiologically necessary set-points of gene expression, use ligand activated nuclear receptors to coordinate hormonal intercellular communications, and utilize a conserved negative feedback circuit to reset gene expression after the hormonal communication has ended.

1.2.3 LRH-1 in Development

During embryonic development, LRH-1 is a critical factor for expression of stem cell pluripotency genes, without which embryonic stem cells cannot divide. Mice homozygous deficient for LRH-1 die at embryonic day 7 due to decreased expression of OCT4, Nanog, and other LRH-1 target genes (Hinshelwood, Shelton et al. 2005). Later in development, LRH-1 expression becomes confined to the liver, digestive system, and reproductive axis. While LRH-1 is necessary for a number of pathways in reproductive tissues, it does not appear to be essential for normal development and sexual maturation of these tissues. This is in contrast to SF-1, in which SF-1 is not only important for basal gonadal physiology, but SF-1 deficient mice suffer from testicular agenesis (Kim, Li et al. 2010; Allali, Muller et al. 2011; Ferraz-de-Souza, Lin et al. 2011).

1.2.4 Enterohepatic Function of LRH-1

The interplay between LRH-1 function in the liver and intestine is a key example of how LRH-1 follows the three conventions discussed above. In the liver, LRH-1 stimulates the basal expression of cytochrome p450 7a1 (Cyp7a1), and Cyp8b1, the rate-limiting enzymes in bile acid synthesis (Lee, Schmidt et al. 2008). It associates with the adopted orphan nuclear receptor LXR, which upon binding to high concentrations of mono-oxygenated cholesterols, further stimulates the induction of Cyp7a1 to promote the metabolism of excess cholesterol into bile for passage out of the body via feces. Liver specific LRH-1 knockout mice have altered bile acid composition, primarily due to the loss of Cyp8b1 (Lee, Schmidt et al. 2008). In the intestine, LRH-1 stimulates expression of membrane associated bile acid transporter enzymes required for the reabsorption of bile acids after a meal. It does so in partner with the adopted orphan nuclear receptor farnesoid X receptor (FXR), whose ligands are bile acids (Mataki, Magnier et al. 2007). LRH-1 and SHP function in a negative feedback circuit that regulates bile acid synthesis. Re-absorbed bile acids make their way back to the liver, where they activate FXR, increase SHP recruitment to the Cyp7a1 promoter, and lead to SHP binding to LRH-1 and its partnering nuclear receptor LXR to repress bile acid synthesis. This resets the liver for the next meal.

1.2.5 Reproductive Axis Function of LRH-1

In the ovary, LRH-1 controls the expression of enzymes needed for follicle maturation and steroid hormone synthesis. Ovary specific LRH-1 knockout mice are infertile, anovulatory, and have severely reduced serum progesterone levels (Duggavathi, Volle et al. 2008). LRH-1 works in close conjunction with ERα to control gene expression, and establishes a negative feedback system through binding by DAX-1 (Lalli, Melner et al. 1998; Sandhoff and McLean 1999; Zhang, Thomsen et al. 2000; Iyer and McCabe 2004; Sablin, Woods et al. 2008). During follicle maturation, LRH-1 stimulates Cyp19a expression, the rate limiting enzyme in estrogen synthesis. At the end of follicle maturation, in response to the LH surge, DAX-1 activity increases and binds to LRH-1 and ERα to represses the transcriptional programs needed for estradiol synthesis. Within cells of the corpus luteum, the remnant of a ruptured mature follicle, LRH-1 increases expression cyp11b1 and other enzymes needed for progesterone synthesis. Estradiol levels decrease significantly, and progesterone levels rise. Progesterone is required for proper maintenance of the uterus and the implanted oocyte after fertilization.

The ovary and pituitary work together to coordinate the reproductive axis, and LRH-1 is expressed in gonadotropin neurons of the pituitary. Within gonadotropin neurons, LRH-1 functions to stimulate expression of the gonadotropin releasing hormone receptor (GnRHr) and the gonadotropin LH and

follicle stimulating hormone (FSH) subunits (Zheng, Yang et al. 2007). It is unclear whether control of these targets is dynamically modulated by LRH-1, or by any form of negative feedback loops involving SHP or DAX-1. However, it has been shown that expression levels set by LRH-1 are important for physiological output of these hormones by the pituitary.

1.2.6 The Female Estrous Cycle

The role of LRH-1 in the reproductive axis is tightly linked to the female estrous cycle. The estrous cycle is divided into four stages: diestrous, proestrous, estrous, and metestrous (Fig 1.2.6.1) (Thrasher, Clark et al. 1967; Nelson, Felicio et al. 1982). Diestrous is the first stage, it lasts 2-3 days in the mouse, and is the time when dormant small primary oocytes mature into large fluid filled graffian follicles and produce estradiol via LRH-1 targeted pathways. Follicle maturation and estradiol release is driven by a steady rise in serum follicle stimulating hormone (FSH) secreted from the pituitary. At first, small primary and secondary follicles mature independently of FSH stimulation using internal transcriptional programs to drive development. Follicles that mature the fastest become the largest and are termed dominant graffian follicles. These become completely dependent on consistent FSH stimulation to complete maturation. Diestrous ends with dominant graffian follicles completing maturation and serum estradiol and FSH levels peaking. Peak estradiol levels act on the brain to induce the LH surge,

beginning the short phase called proestrous. The LH surge activates LH receptors on dominant follicles and leads to rupture and ovulation. This marks the beginning of estrous, and ruptured follicles become reconstituted into corpus lutea, within which LRH-1 directs the synthesis of progesterone. If ovulation does not result in pregnancy, the corpus luteum degenerates and the animal goes through a short phase of metestrous as the hypothalamic pituitary gonadal axis resets to begin again in diestrous. If ovulation occurs in pregnancy, the corpus lutea continues to support the pregnancy with progesterone.

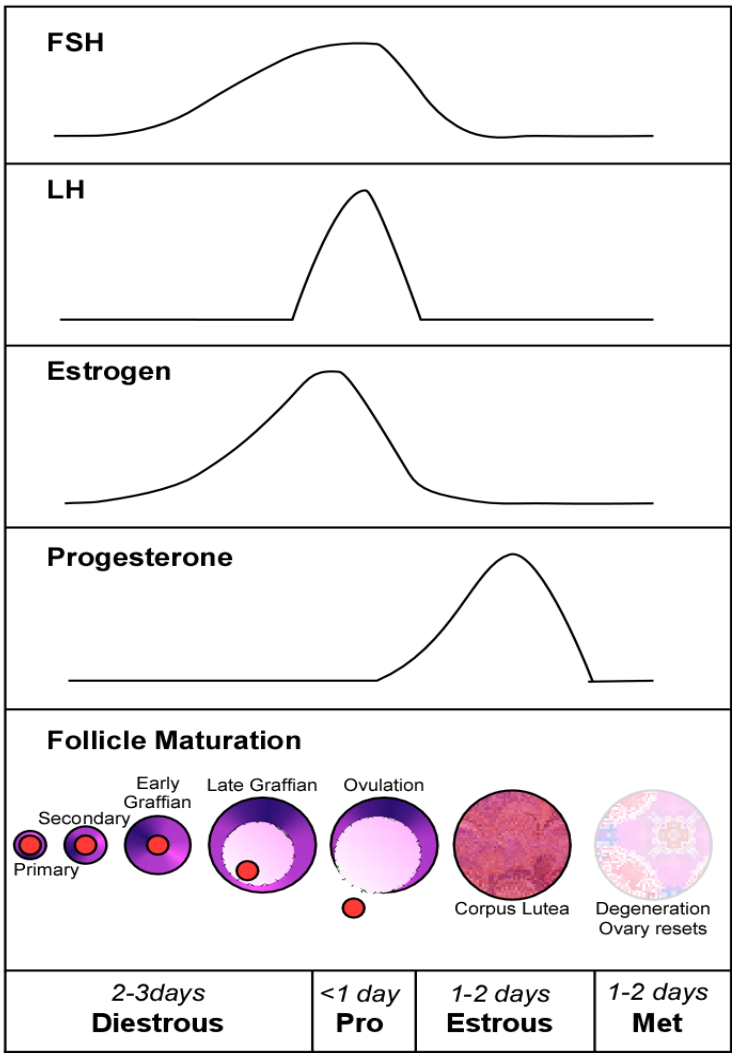

Fig 1.2.6.1: The female estrous cycle. Hormone levels are shown as traces of their serum concentrations. Stages of follicular maturation are depicted as their histological appearance during the estrous cycle. Note that follicles complete maturation at the end of diestrous, and ovulation occurs upon the LH surge in proestrous. Corpus lutea are remnants of ovulated follicles, and secrete progesterone. (Pro: proestrous, Met; metestrous). Adapted from: http://schoolswikipedia.org/wp/m/Menstrual_cycle.htm ; Nelson, J. F., L. S. Felicio, et al. (1982).

1.3. The Hypothalamus

1.3.1 LRH-*1 in the Hypothalamus*

The hypothalamus is a small region of the brain found in almost all species that have a central nervous system. It controls the basic metabolic systems needed an animal's survival. These include body temperature, feeding, energy expenditure, fight or flight mechanisms, pituitary output, mating, and the circadian rhythm. In the mouse, the hypothalamus consists of structures at the base of the brain. In the human, the hypothalamus is in the center of the brain between the thalamus and the brain stem. Hypothalamus structures consist of distinct bundles of neuron cell bodies. These bundles are termed "nuclei"; not to be confused with the nucleus of a cell. Their names describe their approximate location within the brain. Each nucleus of the hypothalamus is responsible for controlling a different basal function in the animal. GnRH neurons, found in the medial preoptic nucleus of the hypothalamus (meaning they are medial to the 3rd ventricle, and rostral to the optic chiasm), control the release of FSH and LH by the pituitary.

The arcuate nucleus (Arc) of the hypothalamus, so named because in humans and rodents its fibers arc along the base of the brain through a structure called the median eminence, contains a few thousand neurons (Fig 1.3.1.1) (Fu and Watson 2012). It is also referred to as the infundibular nucleus in humans

because of its characteristic inverted funnel shape. These neurons are classified into four types based on the predominant peptide secreted at their axon terminal (van den Top and Spanswick 2006). The neuropeptide-Y/agouti-related peptide (NPY/AgRP), and the α-melanocyte stimulating hormone/pro-opiomelanocortin (α-MSH/POMC) neurons control food intake and energy expenditure (Pinto, Roseberry et al. 2004; Coppari, Ichinose et al. 2005; Parton, Ye et al. 2007). Their fibers interface with higher cortical centers in the hypothalamus and indirectly modulate sympathetic/parasympathetic nervous system output to initiate hunger/satiety cues and modulate gut metabolism (Dampney 2011). The tyrosine hydroxylase (Th) neurons synthesize dopamine and send their fibers into the posterior pituitary to control prolactin release. Lastly, the kisspeptin (KISS1) neurons send their fibers to the GnRH neurons in the medial preoptic nucleus, and work to set GnRH neuron pulse generation and output needed for proper FSH and LH release (Gottsch, Popa et al. 2011; Yeo and Herbison 2011).

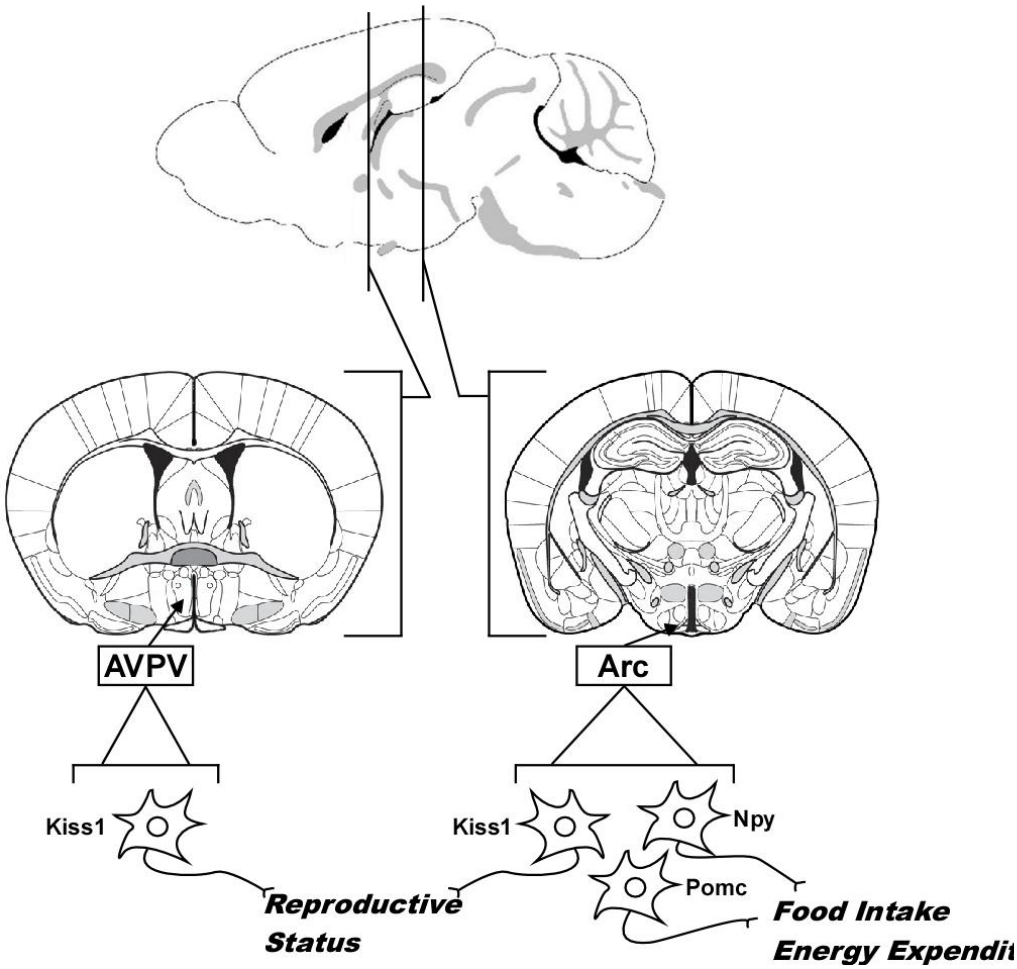

Fig 1.3.1.1 The hypothalamus of the mouse brain. Sagittal section of the mouse brain showing coronal slices of levels containing the AVPV and arcuate nucleus (Arc). Within the Arc, NPY and POMC neurons control food intake and energy expenditure, while KISS1 neurons in the AVPV and Arc control the status of the reproductive axis. Author's rendering with images roughly adapted from: http://www.brain-map.org/

1.3.2 NPY and POMC Neurons

The NPY and POMC neurons are arranged in a circuit that responds to peripheral satiety hormones to regulate food intake. The primary mechanism allowing them to sense satiety levels is expression of the leptin receptor, a tyrosine kinase class transmembrane receptor (Elmquist, Elias et al. 1999; Elmquist 2000; Mirshamsi, Laidlaw et al. 2004; Coppari, Ichinose et al. 2005; Jovanovic and Yeo 2010). Leptin is a hormone released by adipocytes. Peripheral leptin levels decline during hunger. The lack of leptin receptor signaling stimulates synaptic release of NPY. NPY peptide inhibits POMC neuron activity, and the final circuit output leads to autonomic promotion of food seeking behavior. After eating, leptin is released by adipose tissue. Activation of the leptin receptor inhibits NPY release, and stimulates POMC release by POMC neurons. The final output of the circuit under leptin stimulus directs the autonomic nervous system to cease food intake and promote the feelings in the gut of satiety.

The innervation of higher cortical and hypothalamic nuclei such as the paraventricular nucleus and lateral hypothalamic area by NPY and POMC neurons allows them to modulate processes within digestive system organs via autonomic nervous system output. Evidence suggests that these neurons can have some control over liver, intestine, and pancreas endocrinology (Wang, Liu et al. 2004; Chang, Karatayev et al. 2005; Fekete, Singru et al. 2006; Fioramonti, Contie et al. 2007). Recent work has shown that these neurons can directly sense

glucose levels, and may sense free fatty acid levels as well (Hill, Chow et al. 2007; Swierczynski, Goyke et al. 2008). Along with leptin, it is possible these neurons integrate many hormone signals to assess total body nutrient status and coordinate feeding and energy output with enterohepatic physiology.

1.3.3 Kisspeptin Neurons

A fundamental mystery of reproductive biology is the mechanism of how estrogen feeds back on the brain to regulate the reproductive axis. Early in the female estrous cycle, estrogen acts as a negative regulator of GnRH and pituitary hormone release. Yet, once serum estrogen levels peak at the end of diestrous, estrogen becomes a positive regulator of hormone release, leading to ovulation.

Surprisingly, estrogen receptor α (ERα) is not expressed in GnRH neurons or pituitary gonadotropin cells. The mechanism of how estrogen exerts control over the hypothalamic pituitary axis remained a mystery for many years until a breakthrough came in 2001 with the discovery of the kisspeptin neuron (Kotani, Detheux et al. 2001). Kisspeptin neurons are found in the hypothalamus, and are now known to be the target for estrogen's feedback on the brain (Gottsch, Cunningham et al. 2004; Han, Gottsch et al. 2005; Messager, Chatzidaki et al. 2005). Humans with mutations in the kisspeptin gene (*Kiss1*), or mice homozygous deficient for *Kiss1*, are infertile (d'Anglemont de Tassigny, Fagg et al. 2007; Topaloglu, Tello et al. 2012). *Kiss1* is a direct target of ERα, and *Kiss1*

specific ERα KO mice are infertile and suffer from a polycystic ovarian phenotype (Roa, Vigo et al. 2008; Gottsch, Navarro et al. 2009; Mayer, Acosta-Martinez et al. 2010; Mayer and Boehm 2011). Secretion of KISS1 peptide activates its cognate G-protein coupled receptor, GPR54, on gonadotropin releasing hormone (GnRH) neurons, which directs the pituitary to release FSH and LH (Messager, Chatzidaki et al. 2005; Semple, Achermann et al. 2005; Shahab, Mastronardi et al. 2005). Kisspeptin neurons are found in two regions of the hypothalamus, the anteroventral periventricular nucleus (AVPV), and the Arc (Fig 1.3.3.1). These two pools play coordinated but opposite roles in the female brain's response to estrogen (Clarkson, d'Anglemont de Tassigny et al. 2009). While it is well understood that the AVPV pool of KISS1 neurons is responsible for the LH surge, it is unknown how in diestrous kiss1 neurons in the AVPV or Arc work to set the level of FSH release needed for follicle maturation (Maeda, Ohkura et al. 2010). In the AVPV, the peak estrogen in proestrous positively activates *Kiss1* expression and elicits the LH surge. In contrast, the peak estrogen represses Arc *Kiss1* expression. It is thought that Arc neurons somehow set the basal amplitude of FSH pulsatility, and that repression by estrogen during proestrous is responsible for the fall of FSH after ovulation. This is a model that has never been proven, and the mechanism by which Arc KISS1 neurons could set FSH tone is unknown.

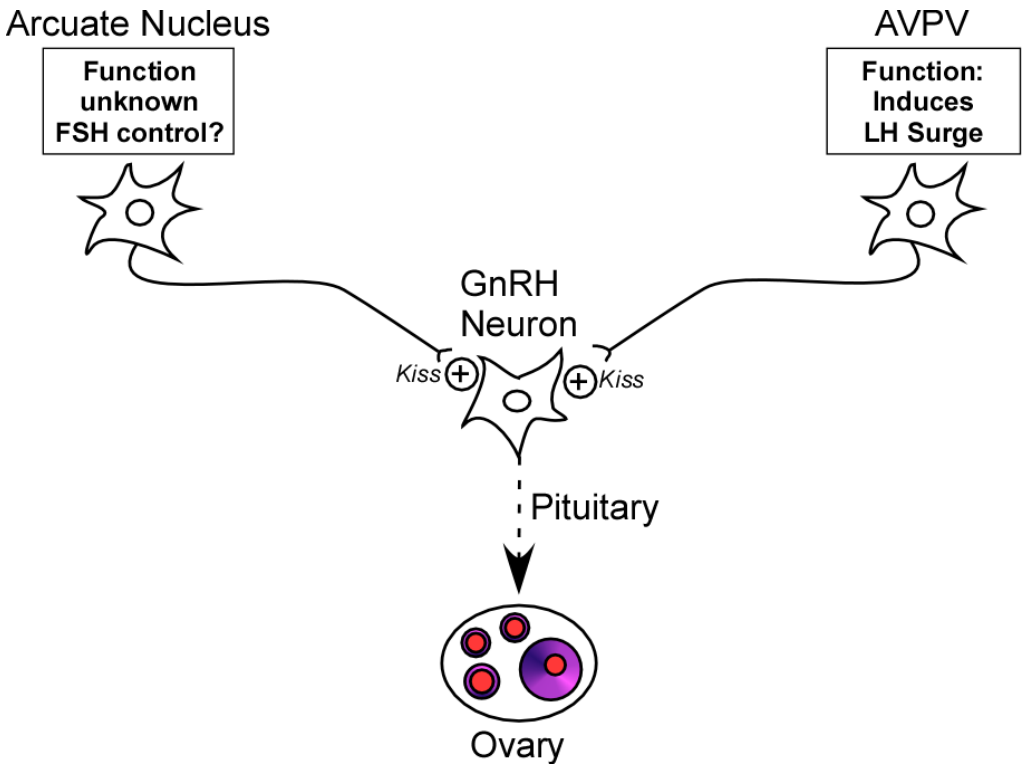

Fig 1.3.3.1: Kisspeptin neuron circuit system in the hypothalamus. KISS1 neurons are found in the AVPV and Arc of the hypothalamus. KISS1 neurons in the AVPV are known to control the LH surge. When serum estrogen levels peak at the end of diestrous, ERα is activated in Kiss1 neurons of the AVPV to elicit a surge of *Kiss1* expression, causing a surge of GnRH and the subsequent LH surge from the pituitary. The role of KISS1 neurons in the Arc is unknown. They do not surge, and *Kiss1* expression is inhibited by ERα activation. It is thought that KISS1 neurons in the Arc control FSH output to stimulate follicular development and estrogen secretion during diestrous, but data are currently lacking to support this hypothesis.

1.4. Dissertation Goals

1.4.1 Justification for Study of LRH-1 in the Hypothalamus

Lrh-1 expression has been observed in the adult human and mouse arcuate nucleus of the hypothalamus (Higashiyama, Kinoshita et al. 2007). A role for LRH-1 in the adult brain has not been established. Our lab has previously studied the role of LRH-1 in the liver and pancreas, and investigators at UT Southwestern have worked with our lab to study the role of LRH-1 in the ovary. A member of our lab, Angie Bookout, set out to determine the expression pattern of all 49 nuclear receptors in the various nuclei of the hypothalamus. These data independently demonstrated that *Lrh-1* was almost exclusively expressed in the Arc. At the time of this dissertation, it was unknown what neuron type within the Arc *Lrh-1* was expressed in, and no role for LRH-1 in the Arc had been suggested.

LRH-1 is an important factor in the enterohepatic system and the ovary. A major theme of LRH-1 biology has been its co-expression in tissues that are interrelated by a common metabolic process. NPY and POMC neurons interface with liver, intestine, and pancreas biology through the autonomic nervous system. Kisspeptin neurons control pituitary gonadotropin function by interfacing with GnRH neurons. I hypothesized that LRH-1 might function in one of these neuron pools within the Arc to exert hypothalamic control over the enterohepatic system,

or the reproductive axis. If this were true, it would demonstrate that *Lrh-1* is expressed at all levels of these axes to ensure hormonal coordination between cells in the central nervous system and peripheral target organs. To this end, I began this project by setting out to determine which neuron pool *Lrh-1* was expressed in, as this would partly dictate its function. From these data, I generated neuron specific *Lrh-1* knockout mice, and LRH-1 transgenic mice, to determine the function of LRH-1 in the neuron pool it was expressed in. Some of these mouse lines had remarkable phenotypes, and allowed us to conclusively determine the overall role of LRH-1 in the Arc and its control of peripheral organ function.

1.4.2 Dissertation Overview

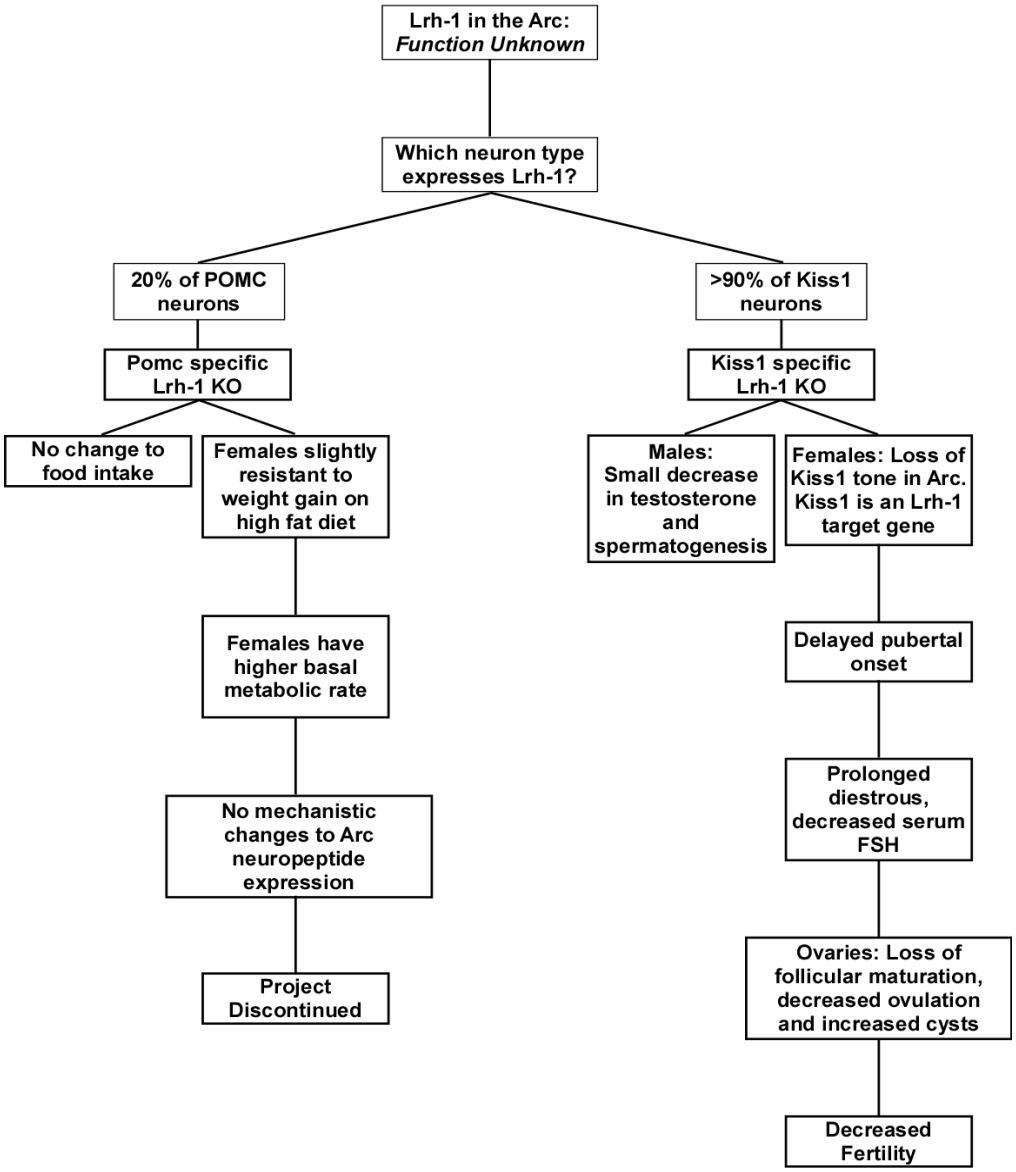

Fig 1.4.2.1 Dissertation overview. This dissertation presents two LRH-1 centric projects. The POMC specific *Lrh-1* KO mouse project, and the female KISS1 specific *Lrh-1* KO mouse project, the latter being the primary support of this degree.

This dissertation will first present data showing which neuron pool *Lrh-1* is expressed in within the Arc. It will present the basal expression patterns of *Lrh-1* during times of high fat diet, during the estrous cycle, and in response to exogenous estrogen and leptin. These experiments helped to elucidate the basic role of LRH-1 in the Arc.

The dissertation will then cover phenotypes of mouse lines generated in which *Lrh-1* was specifically deleted from KISS1 or POMC neurons. It will also cover the findings from a KISS1 specific *Lrh-1* transgenic mouse line. Studies in males and females were undertaken when gender specific differences were expected, and gender specific phenotypes in our mouse lines are discussed. After mouse lines allowed us to determine the probable target genes of LRH-1, the interaction of LRH-1 with the promoters of these genes was studied *in vitro.* These studies were influential in discovering the mechanism by which LRH-1 exerts its action within the neurons it is expressed in.

Throughout this dissertation I will also discuss the evidence I gathered concerning the role of DAX-1 in the Arc. Like LRH-1, DAX-1 is found only in KISS1 neurons of the Arc, and not in those of the AVPV. Its expression also follows that of LRH-1 under a number of different reproductive conditions. Since DAX-1 represses LRH-1 pathways in the ovary, I hypothesized that DAX-1 may be the key factor that is responsible for estrogen's repression of *Kiss1* expression in the Arc. Indeed, at the end of this dissertation I will discuss *in vitro* data

demonstrating that DAX-1 can bind to LRH-1 and inhibit its induction of the *Kiss1* promoter. The next step of research into how these nuclear receptors function in KISS1 neurons would be creation of a KISS1 specific *Dax-1* KO mouse. A Dax-1$^{lox/lox}$ mouse line does not exist or I would have crossed this mouse line myself. Therefore while I present the data here, I will only try to fold its activity into a greater unifying model at the end of this dissertation in the Chapter 6 in the closing remarks and future directions section. Regardless, the study of DAX-1 is the next logical step for this dissertation project, as it very well could be the factor which it explains how estrogen can be repressive to the Arc population of KISS1 neurons, but stimulatory to the AVPV population. At the moment, this conundrum is one of the most elusive and difficult questions in the field of reproductive biology.

The most important finding of this dissertation is the role of LRH-1 in kisspeptin neurons of the female mouse. These data show that kisspeptin is a direct target gene of LRH-1, and LRH-1 functions to set a basal expression level of *Kiss1* that is needed for physiologic output of FSH by the pituitary. In the absence of this set-point in KO mice, pituitary FSH output is not maintained, and ovarian follicles cannot complete maturation and ovulate. These findings are not only important for understanding the role of LRH-1; they offer a compelling explanation for how KISS1 neurons in the Arc control FSH output. While it is well understood how kisspeptin neurons work to elicit the LH surge, it is

unknown how they support and maintain consistent pituitary FSH output. This study demonstrates that kisspeptin neurons in the Arc utilize LRH-1 to set a basal level of *Kiss1* expression to maintain the amplitude of FSH secretion from the pituitary. Much like in other organs, LRH-1 associates with ERα here to control overall *Kiss1* gene function. LRH-1 sets the basal tone of *Kiss1* expression, and ERα represses this basal level to reduce FSH secretion after ovulation. This dissertation concludes that LRH-1 functions across the entire reproductive axis, in the hypothalamus, pituitary, and ovary, to coordinate hormonal actions in cells and the gene output necessary for proper reproductive function and fertility.

References

Allali, S., J. B. Muller, et al. (2011). "Mutation analysis of NR5A1 encoding steroidogenic factor 1 in 77 patients with 46, XY disorders of sex development (DSD) including hypospadias." PLoS One **6**(10): e24117.

Chang, G. Q., O. Karatayev, et al. (2005). "Glucose injection reduces neuropeptide Y and agouti-related protein expression in the arcuate nucleus: a possible physiological role in eating behavior." Brain Res Mol Brain Res **135**(1-2): 69-80.

Chawla, A., J. J. Repa, et al. (2001). "Nuclear receptors and lipid physiology: opening the X-files." Science **294**(5548): 1866-1870.

Clarkson, J., X. d'Anglemont de Tassigny, et al. (2009). "Distribution of kisspeptin neurones in the adult female mouse brain." J Neuroendocrinol **21**(8): 673-682.

Coppari, R., M. Ichinose, et al. (2005). "The hypothalamic arcuate nucleus: a key site for mediating leptin's effects on glucose homeostasis and locomotor activity." Cell Metab **1**(1): 63-72.

d'Anglemont de Tassigny, X., L. A. Fagg, et al. (2007). "Hypogonadotropic hypogonadism in mice lacking a functional Kiss1 gene." Proc Natl Acad Sci U S A **104**(25): 10714-10719.

Dampney, R. A. (2011). "Arcuate nucleus - a gateway for insulin's action on sympathetic activity." J Physiol **589**(Pt 9): 2109-2110.

Denson, L. A., E. Sturm, et al. (2001). "The orphan nuclear receptor, shp, mediates bile acid-induced inhibition of the rat bile acid transporter, ntcp." Gastroenterology **121**(1): 140-147.

Duggavathi, R., D. H. Volle, et al. (2008). "Liver receptor homolog 1 is essential for ovulation." Genes Dev **22**(14): 1871-1876.

Ellinger-Ziegelbauer, H., A. K. Hihi, et al. (1994). "FTZ-F1-related orphan receptors in Xenopus laevis: transcriptional regulators differentially expressed during early embryogenesis." Mol Cell Biol **14**(4): 2786-2797.

Elmquist, J. K. (2000). "Anatomic basis of leptin action in the hypothalamus." Front Horm Res **26**: 21-41.

Elmquist, J. K., C. F. Elias, et al. (1999). "From lesions to leptin: hypothalamic control of food intake and body weight." Neuron **22**(2): 221-232.

Fayard, E., J. Auwerx, et al. (2004). "LRH-1: an orphan nuclear receptor involved in development, metabolism and steroidogenesis." Trends Cell Biol **14**(5): 250-260.

Fekete, C., P. S. Singru, et al. (2006). "Differential effects of central leptin, insulin, or glucose administration during fasting on the hypothalamic-pituitary-thyroid axis and feeding-related neurons in the arcuate nucleus." Endocrinology **147**(1): 520-529.

Fernandez-Marcos, P. J., J. Auwerx, et al. (2011). "Emerging actions of the nuclear receptor LRH-1 in the gut." Biochim Biophys Acta **1812**(8): 947-955.

Ferraz-de-Souza, B., L. Lin, et al. (2011). "Steroidogenic factor-1 (SF-1, NR5A1) and human disease." Mol Cell Endocrinol **336**(1-2): 198-205.

Fioramonti, X., S. Contie, et al. (2007). "Characterization of glucosensing neuron subpopulations in the arcuate nucleus: integration in neuropeptide Y and pro-opio melanocortin networks?" Diabetes **56**(5): 1219-1227.

Fu, Y. H. and C. Watson (2012). "The Arcuate Nucleus of the C57BL/6J Mouse Hindbrain Is a Displaced Part of the Inferior Olive." Brain Behav Evol **79**(3): 191-204.

Gao, D. M., L. F. Wang, et al. (2006). "Expression of mouse liver receptor homologue 1 in embryonic stem cells is directed by a novel promoter." FEBS Lett **580**(7): 1702-1708.

Gottsch, M. L., M. J. Cunningham, et al. (2004). "A role for kisspeptins in the regulation of gonadotropin secretion in the mouse." Endocrinology **145**(9): 4073-4077.

Gottsch, M. L., V. M. Navarro, et al. (2009). "Regulation of Kiss1 and dynorphin gene expression in the murine brain by classical and nonclassical estrogen receptor pathways." J Neurosci **29**(29): 9390-9395.

Gottsch, M. L., S. M. Popa, et al. (2011). "Molecular properties of Kiss1 neurons in the arcuate nucleus of the mouse." Endocrinology **152**(11): 4298-4309.

Han, S. K., M. L. Gottsch, et al. (2005). "Activation of gonadotropin-releasing hormone neurons by kisspeptin as a neuroendocrine switch for the onset of puberty." J Neurosci **25**(49): 11349-11356.

Helsen, C., S. Kerkhofs, et al. (2012). "Structural basis for nuclear hormone receptor DNA binding." Mol Cell Endocrinol **348**(2): 411-417.

Higashiyama, H., M. Kinoshita, et al. (2007). "Expression profiling of liver receptor homologue 1 (LRH-1) in mouse tissues using tissue microarray." J Mol Histol **38**(1): 45-52.

Hill, R. A., J. Chow, et al. (2007). "Fas/FasL-mediated apoptosis in the arcuate nucleus and medial preoptic area of male ArKO mice is ameliorated by selective estrogen

receptor alpha and estrogen receptor beta agonist treatment, respectively." Mol Cell Neurosci **36**(2): 146-157.
Hinshelwood, M. M., J. J. Repa, et al. (2003). "Expression of LRH-1 and SF-1 in the mouse ovary: localization in different cell types correlates with differing function." Mol Cell Endocrinol **207**(1-2): 39-45.
Hinshelwood, M. M., J. M. Shelton, et al. (2005). "Temporal and spatial expression of liver receptor homologue-1 (LRH-1) during embryogenesis suggests a potential role in gonadal development." Dev Dyn **234**(1): 159-168.
Iyer, A. K. and E. R. McCabe (2004). "Molecular mechanisms of DAX1 action." Mol Genet Metab **83**(1-2): 60-73.
Jovanovic, Z. and G. S. Yeo (2010). "Central leptin signalling: beyond the arcuate nucleus." Auton Neurosci **156**(1-2): 8-14.
Kim, K. W., S. Li, et al. (2010). "CNS-specific ablation of steroidogenic factor 1 results in impaired female reproductive function." Mol Endocrinol **24**(6): 1240-1250.
Kotani, M., M. Detheux, et al. (2001). "The metastasis suppressor gene KiSS-1 encodes kisspeptins, the natural ligands of the orphan G protein-coupled receptor GPR54." J Biol Chem **276**(37): 34631-34636.
Kudo, T. and S. Sutou (1997). "Molecular cloning of chicken FTZ-F1-related orphan receptors." Gene **197**(1-2): 261-268.
Lalli, E., M. H. Melner, et al. (1998). "DAX-1 blocks steroid production at multiple levels." Endocrinology **139**(10): 4237-4243.
Lazarus, K. A., D. Wijayakumara, et al. (2012). "Therapeutic potential of Liver Receptor Homolog-1 modulators." J Steroid Biochem Mol Biol.
Lee, Y. K., Y. H. Choi, et al. (2006). "Phosphorylation of the hinge domain of the nuclear hormone receptor LRH-1 stimulates transactivation." J Biol Chem **281**(12): 7850-7855.
Lee, Y. K. and D. D. Moore (2008). "Liver receptor homolog-1, an emerging metabolic modulator." Front Biosci **13**: 5950-5958.
Lee, Y. K., D. R. Schmidt, et al. (2008). "Liver receptor homolog-1 regulates bile acid homeostasis but is not essential for feedback regulation of bile acid synthesis." Mol Endocrinol **22**(6): 1345-1356.
Liu, D. L., W. Z. Liu, et al. (2003). "Expression and functional analysis of liver receptor homologue 1 as a potential steroidogenic factor in rat ovary." Biol Reprod **69**(2): 508-517.
Maeda, K., S. Ohkura, et al. (2010). "Neurobiological mechanisms underlying GnRH pulse generation by the hypothalamus." Brain Res **1364**: 103-115.
Makishima, M., A. Y. Okamoto, et al. (1999). "Identification of a nuclear receptor for bile acids." Science **284**(5418): 1362-1365.
Mangelsdorf, D. J. and R. M. Evans (1995). "The RXR heterodimers and orphan receptors." Cell **83**(6): 841-850.
Margolis, R. N. (2008). "The Nuclear Receptor Signaling Atlas: catalyzing understanding of thyroid hormone signaling and metabolic control." Thyroid **18**(2): 113-122.
Mataki, C., B. C. Magnier, et al. (2007). "Compromised intestinal lipid absorption in mice with a liver-specific deficiency of liver receptor homolog 1." Mol Cell Biol **27**(23): 8330-8339.

Mayer, C., M. Acosta-Martinez, et al. (2010). "Timing and completion of puberty in female mice depend on estrogen receptor alpha-signaling in kisspeptin neurons." Proc Natl Acad Sci U S A **107**(52): 22693-22698.

Mayer, C. and U. Boehm (2011). "Female reproductive maturation in the absence of kisspeptin/GPR54 signaling." Nat Neurosci **14**(6): 704-710.

McEwan, I. J. and A. M. Nardulli (2009). "Nuclear hormone receptor architecture - form and dynamics: The 2009 FASEB Summer Conference on Dynamic Structure of the Nuclear Hormone Receptors." Nucl Recept Signal **7**: e011.

Messager, S., E. E. Chatzidaki, et al. (2005). "Kisspeptin directly stimulates gonadotropin-releasing hormone release via G protein-coupled receptor 54." Proc Natl Acad Sci U S A **102**(5): 1761-1766.

Mirshamsi, S., H. A. Laidlaw, et al. (2004). "Leptin and insulin stimulation of signalling pathways in arcuate nucleus neurones: PI3K dependent actin reorganization and KATP channel activation." BMC Neurosci **5**: 54.

Nelson, J. F., L. S. Felicio, et al. (1982). "A longitudinal study of estrous cyclicity in aging C57BL/6J mice: I. Cycle frequency, length and vaginal cytology." Biol Reprod **27**(2): 327-339.

Ortlund, E. A., Y. Lee, et al. (2005). "Modulation of human nuclear receptor LRH-1 activity by phospholipids and SHP." Nat Struct Mol Biol **12**(4): 357-363.

Out, C., J. Hageman, et al. (2011). "Liver receptor homolog-1 is critical for adequate up-regulation of Cyp7a1 gene transcription and bile salt synthesis during bile salt sequestration." Hepatology **53**(6): 2075-2085.

Parton, L. E., C. P. Ye, et al. (2007). "Glucose sensing by POMC neurons regulates glucose homeostasis and is impaired in obesity." Nature **449**(7159): 228-232.

Pinto, S., A. G. Roseberry, et al. (2004). "Rapid rewiring of arcuate nucleus feeding circuits by leptin." Science **304**(5667): 110-115.

Roa, J., E. Vigo, et al. (2008). "Opposite roles of estrogen receptor (ER)-alpha and ERbeta in the modulation of luteinizing hormone responses to kisspeptin in the female rat: implications for the generation of the preovulatory surge." Endocrinology **149**(4): 1627-1637.

Sablin, E. P., I. N. Krylova, et al. (2003). "Structural basis for ligand-independent activation of the orphan nuclear receptor LRH-1." Mol Cell **11**(6): 1575-1585.

Sablin, E. P., A. Woods, et al. (2008). "The structure of corepressor Dax-1 bound to its target nuclear receptor LRH-1." Proc Natl Acad Sci U S A **105**(47): 18390-18395.

Sandhoff, T. W. and M. P. McLean (1999). "Repression of the rat steroidogenic acute regulatory (StAR) protein gene by PGF2alpha is modulated by the negative transcription factor DAX-1." Endocrine **10**(1): 83-91.

Semple, R. K., J. C. Achermann, et al. (2005). "Two novel missense mutations in g protein-coupled receptor 54 in a patient with hypogonadotropic hypogonadism." J Clin Endocrinol Metab **90**(3): 1849-1855.

Shahab, M., C. Mastronardi, et al. (2005). "Increased hypothalamic GPR54 signaling: a potential mechanism for initiation of puberty in primates." Proc Natl Acad Sci U S A **102**(6): 2129-2134.

Swierczynski, J., E. Goyke, et al. (2008). "Acetyl-CoA carboxylase and fatty acid synthase activities in human hypothalamus." Neurosci Lett **444**(3): 209-211.

Takase, M., T. Nakajima, et al. (2000). "FTZ-F1alpha is expressed in the developing gonad of frogs." Biochim Biophys Acta **1494**(1-2): 195-200.

Thrasher, J. D., F. I. Clark, et al. (1967). "Changes in the vaginal epithelial cell cyle in relation to events of the estrous cycle." Exp Cell Res **45**(1): 232-236.

Topaloglu, A. K., J. A. Tello, et al. (2012). "Inactivating KISS1 mutation and hypogonadotropic hypogonadism." N Engl J Med **366**(7): 629-635.

van den Top, M. and D. Spanswick (2006). "Integration of metabolic stimuli in the hypothalamic arcuate nucleus." Prog Brain Res **153**: 141-154.

Wang, R., X. Liu, et al. (2004). "The regulation of glucose-excited neurons in the hypothalamic arcuate nucleus by glucose and feeding-relevant peptides." Diabetes **53**(8): 1959-1965.

Watson, P. J., L. Fairall, et al. (2012). "Nuclear hormone receptor co-repressors: structure and function." Mol Cell Endocrinol **348**(2): 440-449.

Whitby, R. J., S. Dixon, et al. (2006). "Identification of small molecule agonists of the orphan nuclear receptors liver receptor homolog-1 and steroidogenic factor-1." J Med Chem **49**(23): 6652-6655.

Yeo, S. H. and A. E. Herbison (2011). "Projections of arcuate nucleus and rostral periventricular kisspeptin neurons in the adult female mouse brain." Endocrinology **152**(6): 2387-2399.

Zhang, H., J. S. Thomsen, et al. (2000). "DAX-1 functions as an LXXLL-containing corepressor for activated estrogen receptors." J Biol Chem **275**(51): 39855-39859.

Zheng, W., J. Yang, et al. (2007). "Liver receptor homologue-1 regulates gonadotrope function." J Mol Endocrinol **38**(1-2): 207-219.

CHAPTER TWO

LRH-1 is Expressed in KISS1 and POMC Neurons in the Arcuate Nucleus

2.1 Introduction

Previous studies demonstrated that *Lrh-1* was expressed in the arcuate nucleus (Arc) of the mouse hypothalamus (Gofflot, Chartoire et al. 2007; Higashiyama, Kinoshita et al. 2007). I set out to determine what neuron pool within the Arc *Lrh-1* was expressed in, and from there, determine its function. My first goal was to investigate the expression pattern of *Lrh-1* in the mouse brain by developing my own immunohistochemical labeling techniques. To gain insight into which neuron pathway LRH-1 was working in, I then challenged wildtype (WT) mice with a number of feeding conditions, hormone injections, and reproductive axis conditions and assayed for any changes in *Lrh-1* expression. The next task was to determine the neuronal specificity of *Lrh-1* expression. If LRH-1 was found to localize exclusively to one pool of Arc neurons it would be a strong indicator of its physiological function. A number of techniques and mouse lines were developed to answer this, and conclusively answering it took over one year and a half. These experiments clearly demonstrated that *Lrh-1* was not expressed in NPY neurons, was expressed in a subset of POMC neurons, and expressed in the majority of KISS1 neurons. To investigate the role of LRH-1 in POMC and KISS1 neurons, two neuron specific *Lrh-1* knockout mice were

created, a POMC specific *Lrh-1* knockout, and a KISS1 specific *Lrh-1* knockout. The phenotypes and data gathered from these mice will be discussed in subsequent chapters.

2.2 LRH-**1 Expression in the Mouse Brain**

I began this project by first setting out to determine the expression profile of *Lrh-1* in the mouse brain. One option for accomplishing this was antibody-based immunohistochemistry. Another option was radio-labeled nucleotide probe-based in situ hybridization (ISH). Our lab had access to an antibody that sufficiently labeled LRH-1 protein in developing mice. I attempted to immunolabel Lrh-1 protein in adult mouse brain tissue with this antibody. A number of neurons were labeled with a sufficient signal to noise ratio (Fig 2.2.1 A). However, the expression pattern of LRH-1 was unclear due to high background and a low signal to noise ratio of the antibody. Since there was no brain tissue available from adult *Lrh-1* knockout mice to validate the antibody specificity, I was reluctant to rely any further on this option. I then turned to in situ hybridization. Two ISH probes were constructed that targeted the 3'untranslated region of *Lrh-1* mRNA transcripts. These were tested on mouse brain tissue to determine which one had the highest signal to noise ratio (Fig. 2.2.1 B, C). The second probe tested (seen in Fig 2.2.1 C) was chosen as the final probe to use for ISH, and very efficiently labeled *Lrh-1* in ISH performed on free-

floating sections. This probe was used for the rest of the study. *Lrh-1* expression was present in the lateral hypothalamic region, the ependymal cells of the 3rd ventricle, and was highest throughout the rostral to caudal length of the Arc (Figure 2.2.1 D-F). *Lrh-1* labeling patterns matched previously published data and much more conservative than antibody labeling (Gofflot, Chartoire et al. 2007). Data from these probes were carried further, and the probes were eventually validated for their selectivity for *Lrh-1* on brain tissue from KISS1 neuron specific *Lrh-1* knockout mice. *Lrh-1* expression was not found in the AVPV, cortex, hippocampus, cerebellum, or thalamus.

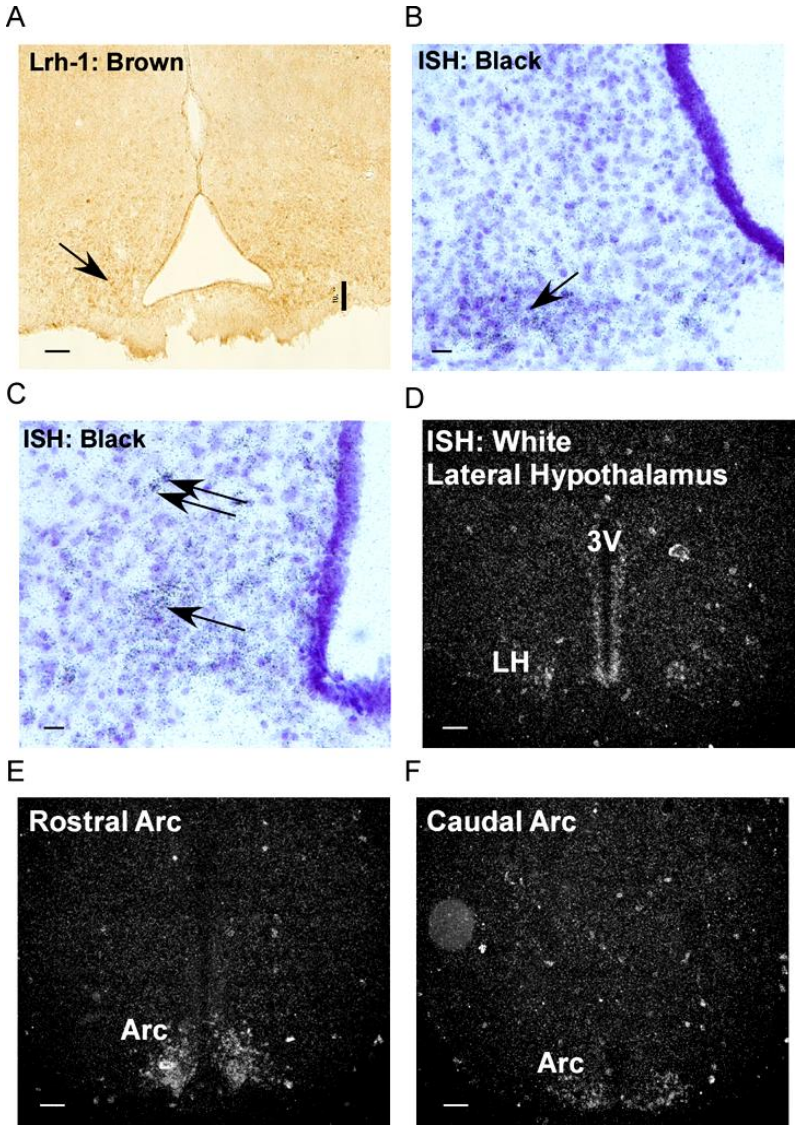

Fig 2.2.1 *Lrh-1* is expressed in the Arc of the hypothalamus. A) Immunohistochemistry for *Lrh-1* on mouse brain tissue developed using diaminobenzoic acid (brown). Arrow denotes Lrh-1 positive neurons (10x magnification, bright field microscopy, scale bar: 100µm, n=3 mice). B,C) *Lrh-1* mRNA specific in situ hybridization probe development. Probe 1 in (B), and Probe 2 in (C) were tested on mouse brains counterstained with thionin (purple). Black granules are more prevalent in Probe 2 and marked with arrows (40x magnification, scale bar: 20µm). D-F) Dark field microscopy of in situ hybridization using probe 2 (10x magnification, scale bar: 100µm).

2.3 *Lrh-1* Expression in Response to Metabolic Challenges

The role of LRH-1 in the Arc was completely unknown. *Npy* and *Pomc* mRNA levels change significantly with dietary challenges, such as fasting, high fat diet (HFD), or leptin injection (Elias, Aschkenasi et al. 1999). *Kiss1* mRNA levels change during puberty, the estrous cycle, and in response to estrogen. *Lrh-1* levels increase in the ovary during folliculogenesis (Gottsch, Navarro et al. 2009; Oakley, Clifton et al. 2009; Gottsch, Popa et al. 2011). With these data in mind, I hypothesized that *Lrh-1* levels might change in the Arc in response to either dietary or reproductive hormones, and that this could offer insight into its neuronal function.

The first experiments focused on the effects of diet treatments and hormones on Arc *Lrh-1* expression. Male C57bl6/J mice were fed a high fat diet (60%kcal from fat) for 8 weeks, sacrificed, and Arc was collected for QPCR measurement of *Lrh-1* mRNA. There was no difference in *Lrh-1* expression in mice on a chow fat diet vs. a high fat diet (Fig 2.3.1 A). I next examined whether the satiety hormone leptin, or the hunger hormone ghrelin, had any effects on Lrh-1 expression. These experiments were done in conjunction with the Joel Elmquist lab. *Lrh-1* expression was measured either via QPCR in dissected Arc samples, or via ISH on brain tissue. Neither leptin administration, nor ghrelin administration, had any effect on *Lrh-1* expression in the Arc (Fig 2.3.1 B-D). These data suggest

that *Lrh-1* expression is not modulated in neurons within the Arc by dietary cues or energy status.

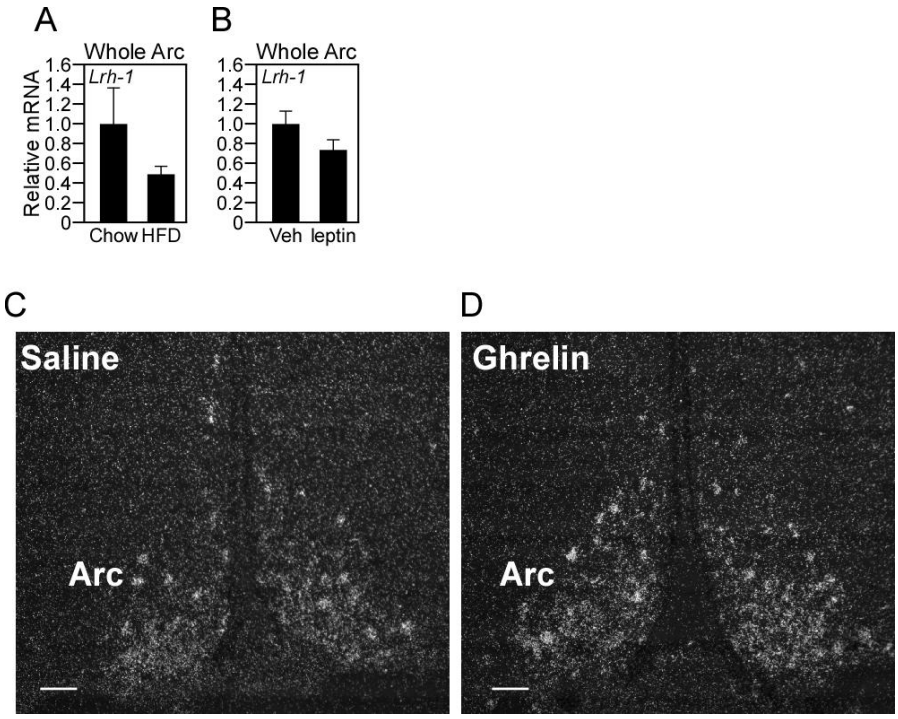

Fig 2.3.1 *Lrh-1* expression in the Arc does not change in response to dietary challenges. A) WT mice were fed either a chow diet or a high fat diet (60%kcal energy from fat) and *Lrh-1* expression measured in Arc by QPCR (n=8 per group). B) WT mice were injected with vehicle, or Leptin, and Arc *Lrh-1* expression was measured (n=6). C) *Lrh-1* expression in mice injected with saline, or Ghrelin (n=3 per group), and perfusion fixed and subjected to in situ hybridization (20x magnification, dark field microscopy, scale bar: 50µm). Error bars represent standard error of the mean.

2.4 *Lrh-1* Expression in Response to Reproductive Axis Conditions

A number of studies were undertaken to test whether *Lrh-1* expression was modulated in response to reproductive axis activity or gonadal hormones. The first experiment focused on whether *Lrh-1* levels changed during pubertal

maturation of the hypothalamus. Arc expression of *Lrh-1* in male and female mice was examined by QPCR before puberty (postnatal day 30, prior to vaginal opening) and after puberty (post natal day 60, after vaginal opening). *Lrh-1* levels doubled by more than two-fold in female mice after puberty, but did not significantly increase in male mice (Fig. 2.4.1 A, B). *Kiss1* expression increased by more than eight-fold in the AVPV after puberty (Fig 2.4.1 C), but like *Lrh-1*, only increased by two-fold in the Arc (Fig 2.4.1 D). Interestingly, *Dax-1* expression increased by 2-fold after puberty in the Arc of females (Fig. 2.4.1 E).

The next experiments examined *Lrh-1* expression changes during the estrous cycle. Estrous cycle stage can be determined by microscopic examination of vaginal epithelia. This procedure allows me to stage many mice quickly and efficiently. Adult female mice were collected in all four stages of the estrous cycle based on vaginal histology. *Lrh-1* expression was measured by QPCR in Arc samples. In adult female mice, *Lrh-1* levels changed substantially over the different phases of the estrous cycle, being highest in diestrous, and dropping during proestrous and estrous (Fig 2.4.1 F). Interestingly, *Kiss1* expression followed a similar trend to *Lrh-1* (Fig 2.4.1 G). This change is consistent with the repressive effects of peak estrogen on *Kiss1* expression during proestrous and estrous. *Dax-1* and *ERα* also had a similar profile albeit not as significant (Fig 2.4.1 H,I). These changes suggested that *Lrh-1* and *Dax-1* expression might be sensitive to estrogen levels in a similar manner to *Kiss1* expression. To test

whether *Lrh-1* expression is susceptible to ERα modulation, female mice were ovariectomized, and after recovery injected with a bolus of estradiol (E2, 6μg per mouse). Ovariectomy substantially increased *Kiss1* expression in the Arc versus sham surgery controls, and E2 injection abrogated this increase (Fig 2.4.1 J). Ovariectomy or E2 injection had no effect on *Lrh-1* expression (Fig 2.4.1 K). However, *Dax-1* expression increased slightly in response to ovariectomy, and was significantly repressed in response to E2 (Fig 2.4.1 L). These data suggest that *Dax-1* expression may be slightly responsive to ERα control or estradiol signaling in the Arc, but *Lrh-1* expression is set independently of estradiol signaling. Some other factor may be responsible for modulating *Lrh-1* levels during the estrous cycle.

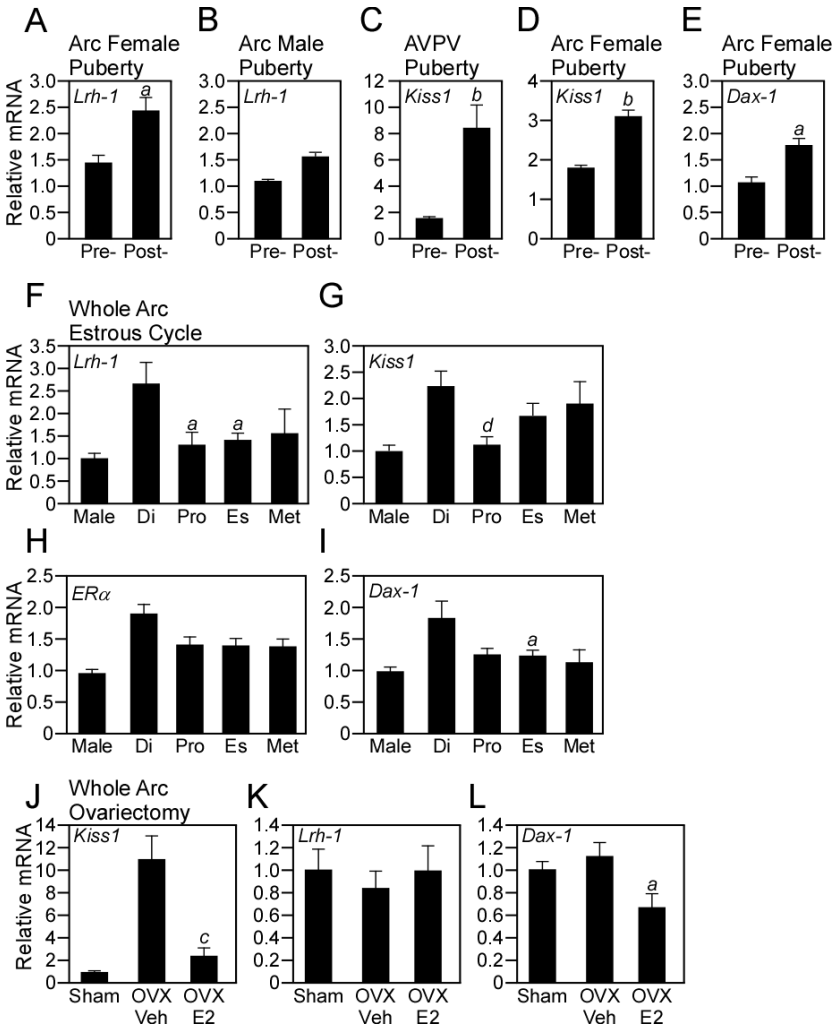

Fig 2.4.1 *Lrh-1* expression in the Arc changes in response to reproductive status. A,B) *Lrh-1* expression increases in the Arc after puberty in female mice (A), but not male mice (B). C) *Kiss1* expression during puberty in the AVPV. D) Arc *Kiss1* expression during puberty. Note the similar fold-change to *Lrh-1*. E) *Dax-1* similarly increases in the Arc during puberty. N=6 mice in both groups for all genes tested. F-I) Expression of *Lrh-1, Kiss1, ERa,* and *Dax-1* in the Arc during the estrous cycle (n=6-10 mice per group). Male mice used as controls. J-L) Effects of ovariectomy and E2 replacement on *Kiss1, Lrh-1,* and *Dax-1* expression in the Arc (n=5 mice per group). Di: Diestrous, Pro: Proestrous, Es: Estrous, Met: metestrous. Error bars represent standard error of the mean. Letters above bars denote statistical significance values (student's T-test): *a*=<.05, *b*=<.01, *c*=<.005, *d*=<.001.

2.5 *Lrh-1* is Expressed in Kiss1 and Pomc Neurons

The next step was to now discern which neuron pool in the Arc expressed *Lrh-1*. The in situ hybridization techniques used to profile *Lrh-1* expression in the mouse brain were combined with immunohistochemistry for markers of NPY, POMC, or KISS1 neurons. Different strategies had to be employed to specifically label each neuronal pool. Antibodies for NPY are not sensitive and thus conventional antibody staining for NPY was not possible. Charlotte Lee and others in the Dr. Elmquist lab were able to supply pre-sectioned RNAse free brain tissue from mice in which the green fluorescent protein (GFP) had been expressed specifically in NPY neurons. Anti-GFP antibodies are readily available, give strong signal to noise ratio, and are extremely specific. This tissue was immuno-labeled for GFP, then labeled with the *Lrh-1* ISH probe (Fig 2.5.1 A). Labeling POMC neurons was done with a β-endorphin specific antibody prior to *Lrh-1* labeling (Fig 2.5.1 B). β-endorphin is a cleavage product of α-MSH in POMC neurons and gives very specific immunohistochemical results. Tyrosine hydroxylase neurons were not examined.

Similar to the strategy employed against NPY neurons, there was no available antibody specific for KISS1 neurons. I was unable to label KISS1 neurons in any capacity compatible with *Lrh-1* ISH until 2009, when Dr. Carol Elias' lab completed the construction of a Kiss1-Cre mouse. Their lab validated the specificity of Cre-recombinase expression by crossing the mouse line with a

Cre-sensitive β-galactosidase (β-gal) reporter mouse. Upon recombination, all KISS1 neurons expressed β-gal, which could be effectively stained using β-gal specific antibodies. As soon as this KISS1 reporter mouse was created, I obtained sectioned brain tissue samples, and labeled them using β-gal antibodies and the *Lrh-1* ISH probe (Fig 2.5.1 C). Images from all three experiments were quantified using conventional microscopy co-localization techniques, and allowed me to determine the expression level of *Lrh-1* in each of the three neuronal pools. Co-localization studies demonstrated that *Lrh-1* was not expressed in NPY neurons, expressed in ~20% of POMC neurons, and expressed in ~90% of KISS1 neurons (Fig. 2.5.1 D).

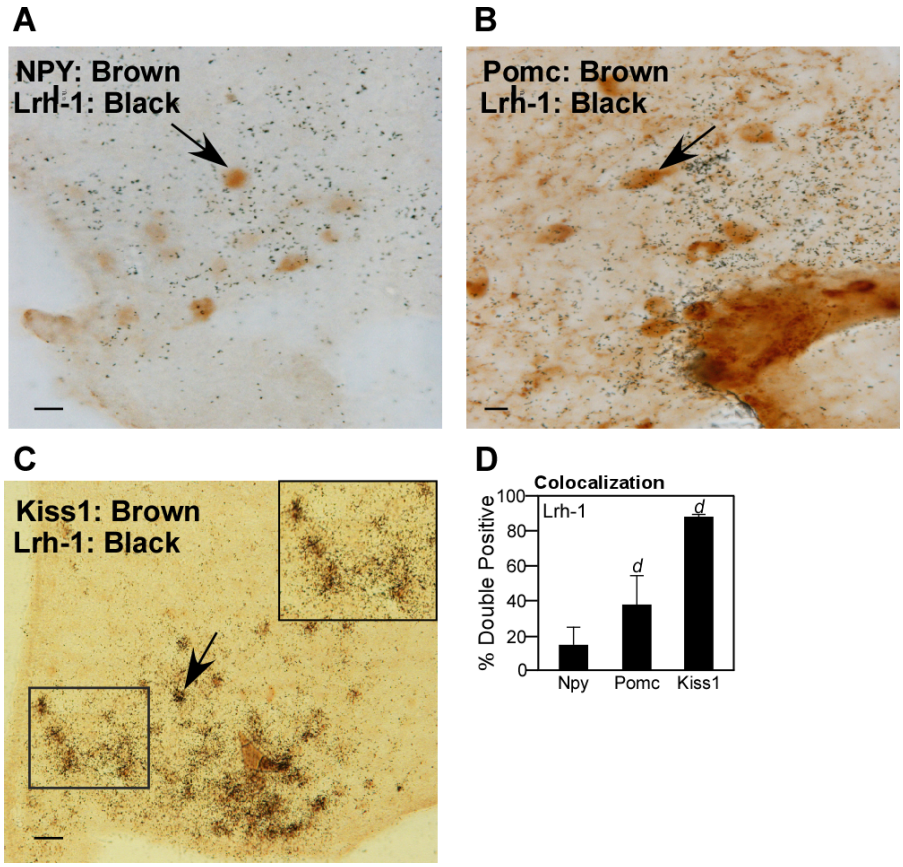

Fig 2.5.1 *Lrh-1* is expressed in KISS1 and POMC neurons in the Arc. A) Dual *Lrh-1* in situ hybridization and immunohistochemistry for NPY neurons. Arrow marks a representative NPY neuron not containing *Lrh-1* signal. B) Dual *Lrh-1* in situ hybridization and POMC neuron immunohistochemistry. Arrow marks a neuron co-localized for both signals. C) Dual *Lrh-1* in situ hybridization and *Kiss1* immunohistochemistry. *Lrh-1* co-localizes with almost all KISS1 neurons (arrows). N=3 mice per stain, all images 40x microscopy, bright field, scale bars: 20µm. D) Quantification of co-localization of both stains in neuronal cell bodies in the Arc. All neurons were manually counted for single or dual labeling (n=3 animals per stain, multiple slides quantified per animal). Error bars represent standard error of the mean. Letters above bars denote statistical significance values (student's T-test): *a*=<.05, *b*=<.01, *c*=<.005, *d*=<.001.

As soon as I observed localization of *Lrh-1* in POMC neurons, I initiated the crossing of a POMC-Cre expressing mouse line with our *Lrh-1*$^{lox/lox}$ mouse line to create a POMC neuron specific *Lrh-1* knockout mouse. Details on this line's phenotype are found in chapter 5. The most interesting results came with the co-localization of *Lrh-1* and *Kiss1*. *Lrh-1* was highly enriched in KISS1 neurons of the Arc, but was not expressed in KISS1 neurons of the AVPV. This was one of the first major molecular differences known between KISS1 neurons at these two sites of the hypothalamus, and became the corner stone of my hypothesis concerning the role of LRH-1 in KISS1 neurons. Shortly after, I crossed our *Lrh-1*$^{lox/lox}$ mouse with the KISS1-Cre mouse. The study of the role of LRH-1 in KISS1 neurons is in chapters 3 and 4.

After completing these experiments, I wanted to develop an independent method of quantifying the expression of *Lrh-1* in these three neuron pools. While the data gathered from immunohistochemical co-localization techniques was reliable and repeatable, it was not strictly quantifiable. I worked with Angie Bookout, and Angela Mobley of the UT Southwestern FACS Core facility to develop a technique in which we could isolate the three different neuronal pools using FACS, and directly measure *Lrh-1* mRNA content via QPCR (Cravo, Margatho et al. 2011). NPY-GFP, POMC-GFP, and KISS1-GFP mouse lines developed by Drs. Elmquist and Elias were used. Arcuate nuclei were dissected away from the brain parenchyma, digested in a weak dispase solution with

manual dissociation, and immediately FACS sorted based on size and complexity (to isolate living single neurons), and GFP fluorescence intensity (to isolate GFP^+, or GFP^- control neurons). From one Arc, we were able to purify between 100-1000 individual neurons. Success depended largely on the resiliency of the neurons and the GFP intensity after dissociation. Only picograms of RNA were actually obtainable from these samples. However, I combined an RNA purification kit used for single cell laser capture micro-dissection with a whole genome pre-amplification kit. This allowed me to efficiently extract the picograms of RNA from the neurons and amplify the RNA signatures to levels high enough to utilize conventional QPCR. This worked surprisingly well. The purity of each neuron pool was verified by QPCR for their respective neuropeptides, and showed that the pools were >90% pure (data not shown). *Lrh-1* mRNA expression was quantified using QPCR. Much like our co-localization results, *Lrh-1* was absent from NPY neurons, present at low levels in POMC neurons, and highly expressed in KISS1 neurons (Fig 2.5.2 A). I did not develop an ISH probe for *Dax-1*, but instead analyzed its expression profile in these FACS samples. Like *Lrh-1*, *Dax-1* was expressed in POMC and KISS1 neurons (Fig 2.5.2 B). All together, these FACS results allowed me to conclude that within the Arc, LRH-1 and DAX-1 are enriched in Kiss1 neurons. Considering the changes in *Lrh-1* and *Dax-1* expression during the various reproductive conditions, these data highly suggested that LRH-1 may play a role in the hypothalamic control of

reproduction, and that it may be controlled by a DAX-1 negative feedback pathway similar to the one in the ovary.

KISS1 neurons are found in two regions of the brain. The previous ISH histology did not show *Lrh-1* in the AVPV, but no ISH was done for *Dax-1*. I examined whether *Lrh-1* and *Dax-1* were expressed in the AVPV by creating a dissection protocol for acutely dissecting and collecting the AVPV. For others in the lab, I also trained myself in dissecting the suprachiasmatic nucleus (SCN), the circadian rhythm generator of the brain. Daisuke Kohno in the Elmquist Lab had previously trained me in dissecting out the Arc, but no methods were known for dissecting out other hypothalamic regions. I used anatomical markers (i.e. location relative to 3rd ventricle, sella turcica, median eminence, optic chiasm, and internal capsule white matter tract) to accurately dissect each brain region. After a few months I could dissect out the AVPV, SCN, and Arc in under a minute, completely negating any possibility of RNA degradation and in terms of my project's needs, pushing laser capture microdissection towards the realm of over-expensive obsolescence. QPCR measurements of *Lrh-1* and *Dax-1* expression showed that they were both confined to the Arc (Fig 2.5.2 C,D). These were extremely important observations, as LRH-1 and DAX-1 became the first known molecular differences between KISS1 neurons at these two sites of the brain.

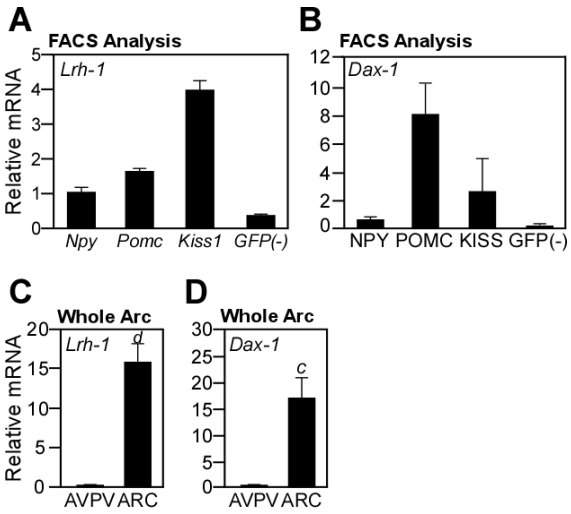

Fig 2.5.2 FACS analysis of *Lrh-1* expression in NPY, POMC, and KISS1 neurons collected from the Arc. A) *Lrh-1* expression quantified by QPCR in collected pools of GFP(+) NPY, POMC, KISS1 neurons, and GFP(-) neurons. B) *Dax*-1 expression in the same samples. N=3 pools of 2 mice in each pool. C,D) Whole AVPV and Arc dissection and analysis of *Lrh-1* and *Dax-1* expression. Both are not expressed in the AVPV (n=10). Error bars represent standard error of the mean. Letters above bars denote statistical significance values (student's T-test): *a*=<.05, *b*=<.01, *c*=<.005, *d*=<.001.

2.6 Discussion

Previously published research indicated that *Lrh-1* was expressed in the Arc, but with unknown function. This dissertation expanded on these observations by determining that *Lrh-1* was expressed in KISS1 and POMC neurons, and that *Lrh-1* expression was responsive to various physiological conditions related to reproduction. *Lrh-1* expression was unchanged by a high fat diet, or satiety or hunger hormone injections. Puberty and the estrous cycle had significant effects on *Lrh-1*, *Dax-1*, and *Kiss1* expression in the Arc.

The most interesting result from these studies came with the co-localization of *Lrh-1* and *Kiss1*. While KISS1 neurons in the Arc were densely labeled for *Lrh-1* mRNA, no *Lrh-1* mRNA was found in the KISS1 neurons of the AVPV. I came to this result only a few weeks after the KISS1-cre mouse completed validation. LRH-1 and DAX-1 became the first known molecular differences between KISS1 neurons at these two sites of the brain. The question became, why was *Lrh-1* and *Dax-1* expressed only in Arc KISS1 neurons, and what did it allow Arc KISS1 neurons to do that AVPV KISS1 neurons couldn't? To so quickly find a gene that was differentially expressed in the two pools of KISS1 neurons was startling to Dr. Elias and me. Soon thereafter the Elias lab discovered many more genes, including the leptin receptor, and cell surface glutamate and GABA channel receptors, that were differentially expressed at these two pools of neurons.

References

Cravo, R. M., L. O. Margatho, et al. (2011). "Characterization of Kiss1 neurons using transgenic mouse models." Neuroscience **173**: 37-56.

Elias, C. F., C. Aschkenasi, et al. (1999). "Leptin differentially regulates NPY and POMC neurons projecting to the lateral hypothalamic area." Neuron **23**(4): 775-786.

Gofflot, F., N. Chartoire, et al. (2007). "Systematic gene expression mapping clusters nuclear receptors according to their function in the brain." Cell **131**(2): 405-418.

Gottsch, M. L., V. M. Navarro, et al. (2009). "Regulation of Kiss1 and dynorphin gene expression in the murine brain by classical and nonclassical estrogen receptor pathways." J Neurosci **29**(29): 9390-9395.

Gottsch, M. L., S. M. Popa, et al. (2011). "Molecular properties of Kiss1 neurons in the arcuate nucleus of the mouse." Endocrinology **152**(11): 4298-4309.

Higashiyama, H., M. Kinoshita, et al. (2007). "Expression profiling of liver receptor homologue 1 (LRH-1) in mouse tissues using tissue microarray." J Mol Histol **38**(1): 45-52.

Oakley, A. E., D. K. Clifton, et al. (2009). "Kisspeptin signaling in the brain." Endocr Rev **30**(6): 713-743.

CHAPTER THREE

The Role of LRH-1 in KISS1 Neurons of Female Mice

3.1 Introduction

My previous experiments determined that LRH-1 was predominately expressed in KISS1 neurons in the arcuate nucleus (Arc). Surprisingly, LRH-1 was not expressed in KISS1 neurons in the AVPV. With what was known of LRH-1 function in the ovary and pituitary, this led me to investigate whether LRH-1 was involved in a transcriptional regulatory system in KISS1 neurons to support ovarian biology and fertility.

KISS1 neurons are master regulators of the hypothalamic pituitary gonadal axis. Humans with mutations in the *Kiss1* gene, or mice homozygous deficient for *Kiss1*, are infertile (Kotani, Detheux et al. 2001; Mayer and Boehm 2011; Topaloglu, Tello et al. 2012). *Kiss1* is a direct target of estrogen receptor α (ERα), and *Kiss1* specific ERα KO mice are infertile and suffer from a polycystic ovarian phenotype (Mayer, Acosta-Martinez et al. 2010). KISS1 neurons are found in two regions of the hypothalamus, the anteroventral periventricular nucleus (AVPV), and the arcuate nucleus (Arc). Secretion of KISS1 peptide activates its cognate G-protein coupled receptor, GPR54, on gonadotropin releasing hormone (GnRH) neurons, which direct the pituitary to release follicle

stimulating hormone (FSH) and luteinizing hormone (LH) (Han, Gottsch et al. 2005; Messager, Chatzidaki et al. 2005). The female estrous cycle begins with diestrous, at which time FSH must be consistently released at adequate concentrations to ensure ovarian follicles mature. In proestrous, follicle maturation completes and follicular secretion of estradiol peaks. The peak estradiol levels activate ERα in KISS1 neurons in the AVPV, increasing *Kiss1* expression and peptide release. This causes pituitary LH secretion to surge to trigger ovulation of the matured follicles. At the same time, ERα activation in KISS1 neurons in the Arc represses *Kiss1* expression. The female is then fertile during estrous. While it is well understood that in proestrous the AVPV pool of Kiss1 neurons is responsible for the LH surge needed for ovulation, it is unknown how in diestrous KISS1 neurons in the AVPV or Arc work to set the tonal level of FSH release needed for follicle maturation. Similarly, besides the role of ERα, very little is known about other possible transcription factors that might work during the estrous cycle to modulate *Kiss1* expression (Mueller, Dietzel et al. 2011).

The findings in this chapter suggest that LRH-1 sets a basal tone of *Kiss1* expression in the Arc that stimulates the requisite levels of FSH secretion from the pituitary needed for follicle maturation. KISS1 specific *Lrh-1* knockout and transgenic mouse models demonstrate that the presence of LRH-1 in KISS1 neurons is critical for the timing of ovulation and maintenance of fertility. Further,

these data suggest that it is this basal LRH-1 dependent stimulation of *Kiss1* expression that molecularly differentiates the Arc from the AVPV. This molecular distinction allows these two pools of neurons to sequentially regulate and time FSH and LH release from the pituitary during the estrous cycle. In chapter 4, I present the experiments that show that *Kiss1* is a direct target gene of LRH-1 *in vivo,* and that it uses a putative LRHRE in the *Kiss1* promoter to activate gene transcription. There was very little to no biologically significant phenotype in male KISS1 specific KO mice and therefore they are not presented in this dissertation.

3.2 Deletion of *Lrh-1* from Kiss1 Neurons

To determine the role of LRH-1 in KISS1 neurons of the Arc, I crossed a previously generated mouse in which exon 5 of the *Lrh-1* gene was flanked by loxp sites (*Lrh-1*$^{lox/lox}$ mouse) with the KISS1-Cre mouse to generate a KISS1 specific *Lrh*-1 knockout mouse (Lee, Schmidt et al. 2008). QPCR of dissected whole Arc tissue, and ISH of female mouse brain slices, demonstrated that *Lrh-1* levels were significantly reduced in the Arc of the knockout (KO) mice (Fig 3.2.1 A-C). A number of neurons, presumably POMC neurons, or Kiss1 neurons not expressing the Cre-recombinase enzyme, still expressed Lrh-1 in the Arc of KO mice. It is possible that there are other LRH-1 expressing neurons that express neither *Pomc* or *Kiss1*. *Cre* mRNA was efficiently expressed in the Arc of KO

mice (Fig 3.2.1 D). *Lrh-1* mRNA levels were unchanged in the pituitary, ovary, and other peripheral tissues (Fig 3.2.1 E-G).

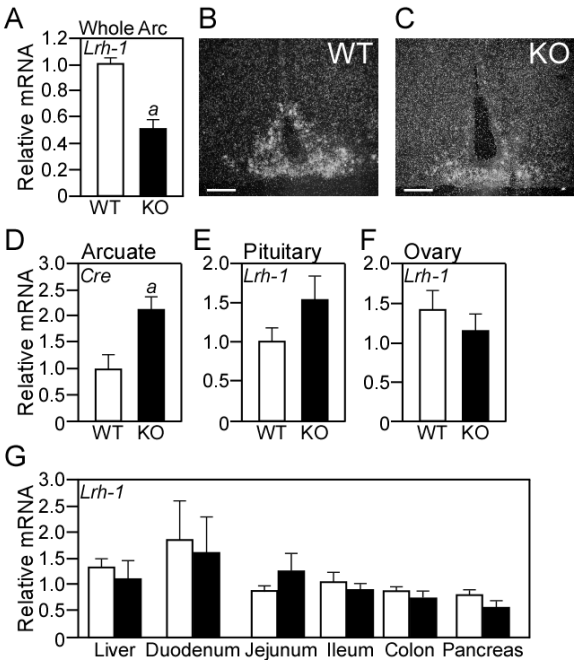

Fig 3.2.1 Generation of KISS1 specific *Lrh-1* knockout (KO) mouse. A) *Lrh-1* mRNA is decreased in whole Arc of KO mice as compared to wildtype (WT) littermates (n=8 per group). B-C) In situ hybridization for *Lrh-1* in Arc of WT (B) and KO (C) mice (dark field microscopy, 20x magnification, scale bars: 50µm). D) *Cre* expression in the Arc of WT and KO mice (n=8). E,F) *Lrh-1* mRNA levels in pituitaries and ovaries (n=8). G) QPCR measurement of *Lrh-1* expression in other LRH-1 target organs (n=8). Error bars represent standard error of the mean. Letters above bars denote statistical significance values (student's T-test): *a*=<.05, *b*=<.01, *c*=<.005, *d*=<.001.

To ensure that KISS1 neurons expressing *Cre* had complete deletion of *Lrh-1* in the Arc of KO mice, I crossed my KO mouse into the Cre-dependent tomato-red fluorescent protein (Td-Tomato) mouse line (Fig 3.2.2 A), resulting in Td-Tomato expression in the KISS1 neurons targeted for *Lrh-1* deletion. This mouse is referred to as the TdT-KO mouse. This mouse efficiently expressed

tomato-red fluorescent protein in KISS1 neurons of the Arc (Fig 3.2.2 B). *Lrh-1*$^{lox/lox}$, Td-Tomato^{+}, KISS1-Cre^{+} mice were used in FACS sorting experiments. *Lrh-1*$^{wt/wt}$, EGFP^{+}, KISS1-Cre^{+} mice were used as WT controls. Both of these mouse lines were generated from the same KISS1-Cre line, and both reporter strains were of C57bl6/j origin, giving the matched EGFP^{+} WT, and Td-Tomato^{+} KO neurons, similar backgrounds. Td-Tomato^{+} neurons collected by FACS were verified as >90% enriched for KISS1 by quantifying their expression of *Npy*, *Pomc*, and *Kiss1* mRNA via QPCR (Fig 3.2.2 C). *Lrh-1* mRNA was quantified via QPCR in the sorted WT EGFP^{+} and Td-Tomato^{+} KO neurons. *Lrh-1* expression was almost undetectable in the Td-Tomato^{+} KO neurons (Fig 3.2.2 D). This quantification was not able to reach statistical significance (student's T-test) because of the scarcity of *Lrh-1*$^{lox/lox}$, Td-Tomato^{+}, KISS1-Cre^{+} mice during this study. However, these FACS experiments clarified that while certain neurons in the Arc still expressed *Lrh-1* in KO mice, near complete deletion of *Lrh-1* was occurring in the KISS1 neurons expressing Cre-recombinase.

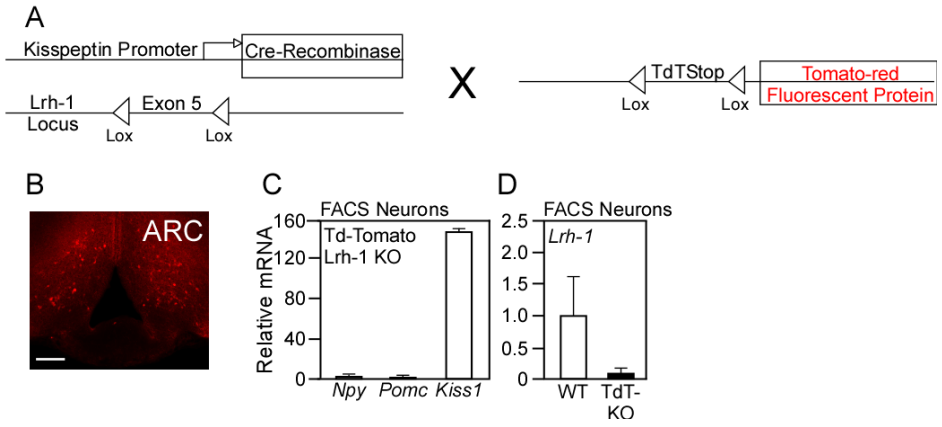

Fig 3.2.2 Tomato-red expressing KISS1 specific *Lrh-1* KO mice (TdT-KO) allow for selective assessment of gene changes in KISS1 neurons. A) Breeding strategy for generation of the reporter mouse line. B) Epifluorescent image of Arc from a female mouse generated from the above breeding strategy (rhodamine filter, 10x magnification, scale bar: 100µm). No immunohistochemistry was needed to visualize tomato-red. C) QPCR analysis of neuropeptide expression in Td-Tomato expressing neurons FACS collected from Arc of the KISS1-Cre^{+}, Td-Tomato^{+}, *Lrh-1*$^{lox/lox}$ TdT-KO reporter line (n=3 animals per group). D) QPCR of *Lrh-1* expression in EGFP WT, and Td-KO neurons collected by FACS (n=3 animals per group). Error bars represent standard error of the mean.

In order to create a potentially useful gain-of-function model for LRH-1 in the Arc, I generated a KISS1 specific *Lrh-1* transgenic mouse line. The transgenic cassette utilized a Cre-removable triple-polyA transcriptional stop signal upstream of the *Lrh-1* transgene (Fig 3.2.3 A)(Fukuda, Scott et al. 2006). Upon *Cre* induction, LoxP recombination removes the transcriptional stop signal, allowing for *Lrh-1* overexpression. Prior to transgenic mouse generation, this transgenic vector was tested in cell culture to verify *Cre*-dependent LRH-1 protein over-expression (Fig 3.2.3 B). Transgenic mice were crossed with the same KISS1-cre mouse used to generate *Lrh-1* KO animals. The resulting mouse line (*Lrh-1* Tg)

had 4-fold over-expression of *Lrh-1* in the Arc (Fig 3.2.3 C). *Lrh-1* expression was unchanged in the pituitary, and ovary of *Lrh-1* Tg mice (Fig 3.2.3 D,E).

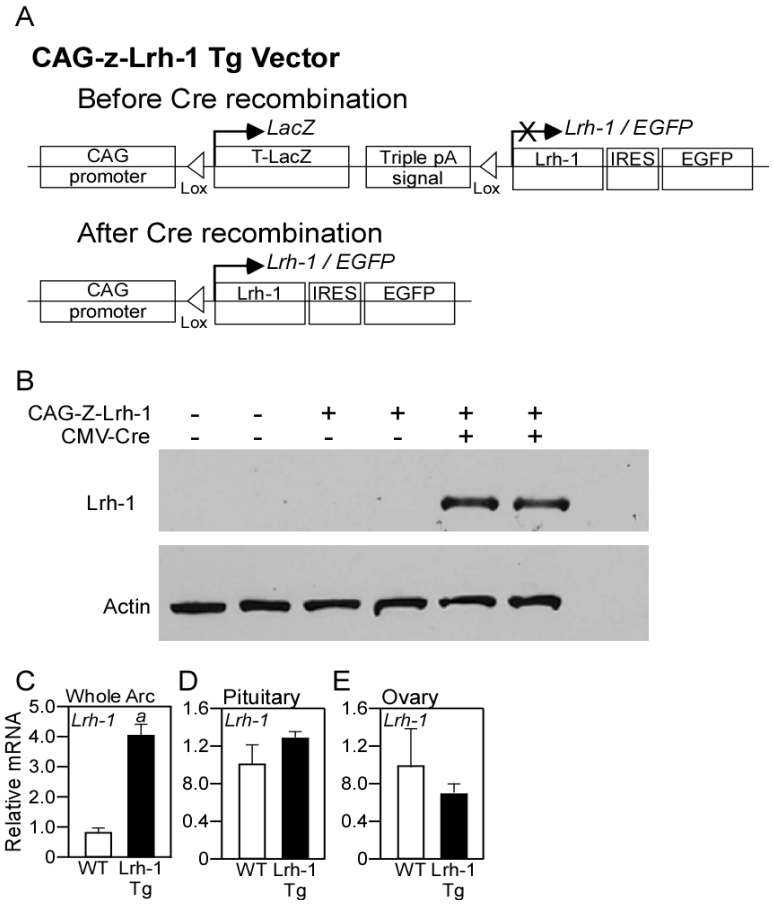

Fig 3.2.3 Generation of the KISS1 specific *Lrh-1* transgenic mouse line (*Lrh-1* Tg). A) Schematic of the CAG-Z-*Lrh-1* transgene cassette. Cre-recombination removes a LacZ-reporter, and the triple polyA transcriptional stop signal. B) Transient transfection of Hek293 cells and western blot assay. LRH-1 protein is only expressed in the presence of Cre expression. C) *Lrh-1* expression by QPCR from dissected whole Arc of the *Lrh-1* Tg line (n=4 per group). D) *Lrh-1* expression is unchanged in the pituitary (n=4). E) *Lrh-1* levels are unchanged in the Ovary (n=4). Error bars represent standard error of the mean. Letters above bars denote statistical significance values (student's T-test): *a*=<.05, *b*=<.01, *c*=<.005, *d*=<.001.

Body weight and body composition by MRI was measured in WT and KO female mice. There was no difference in weight, fat mass, or lean mass, in adult female KO animals (Fig. 3.2.4 A-D).

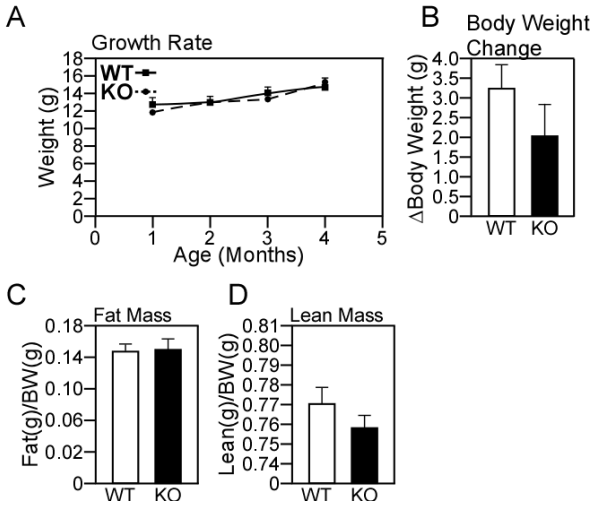

Fig 3.2.4 Body weight and body composition analysis of female KISS1 specific *Lrh-1* KO mice. A,B) There is no difference in growth rate and body weight gain in KO and WT littermates followed for 4 months (n=5-7 per group). C) MRI analysis of fat mass in WT and KO animals. Fat mass is presented normalized to total body weight. D) MRI analysis of lean mass in WT and KO mice, normalized to body weight. Both experiments n=5-7 per group. Error bars represent standard error of the mean.

3.3 Lrh-1 Sets the Basal Tone of Kiss1 Expression

ERα activation represses *Kiss1* expression in the arcuate nucleus, but few other transcription factors have been shown to be important for *Kiss1* transcription. In whole Arc samples dissected from female KO mice, *Kiss1* mRNA levels were significantly reduced in diestrous, and estrous (Fig 3.3.1 A,B). Similarly, *Kiss1* expression assayed by QPCR in FACS collected Td-Tomato^{+} KO

neurons was >2 fold lower than *Kiss1* expression in $EGFP^+$ WT neurons (Fig 3.3.1 C). Importantly, *Kiss1* levels were increased by almost 4-fold in whole Arc samples from *Lrh-1* Tg mice in diestrous (Fig 3.3.1 D). To test the response of KISS1 neurons in the Arc to estrogen in my KO mice, WT and KO mice were ovariectomized, and two weeks later were given an intraperitoneal injection of either vehicle, or estrogen (E2, 6μg/mouse). After ovariectomy, WT and KO mice injected with vehicle experienced a significant increase in *Kiss1* expression in the Arc (Fig 3.3.1 E). This increase in *Kiss1* expression was repressed in ovariectomized WT and KO mice injected with E2. While the ability of E2 to repress *Kiss1* expression was still intact in KO mice, *Kiss1* expression was always significantly lower than in WT counterparts. This strongly suggested that LRH-1 worked to set a basal level of *Kiss1* expression in the Arc, and that this role was independent of the repressive function ERα.

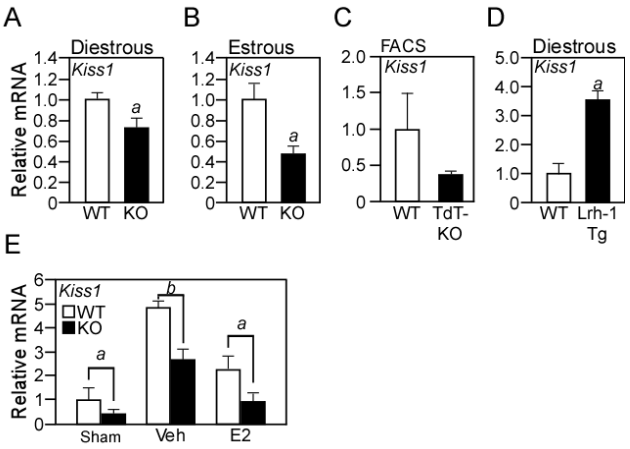

Fig 3.3.1 The basal tone of *Kiss1* expression in the Arc is dependent upon LRH-1. A,B) *Kiss1* expression is significantly decreased in dissected whole Arc of female mice in diestrous, and estrous (n=8, diestrous. n=5, estrous). C) *Kiss1* expression is decreased in FACS collected Td-Tomato KO neurons. D) *Kiss1* expression is significantly increased in whole Arc of *Lrh-1* Tg mice. E) Ovariectomy and either vehicle (Veh), or estradiol (E2) replacement in WT and KO mice. Sham mice represent those where ovaries were kept intact (n=6 per group). Error bars represent standard error of the mean. Letters above bars denote statistical significance values (student's T-test): *a*=<.05, *b*=<.01, *c*=<.005, *d*=<.001.

3.4 *Lrh-1* Deletion from KISS1 Neurons Disrupts the Estrous Cycle

Kisspeptin neuron function in the Arc is known to be required for estrous cycle timing and ovulation (d'Anglemont de Tassigny, Fagg et al. 2007). To test whether the decrease in *Kiss1* expression in the Arc affected female reproductive function, I analyzed pubertal onset, and estrous cycle timing in KO mice. There was no significant difference in the age of vaginal opening in KO females (data not shown). However, while WT mice did experience their first estrous cycle at approximately 60 days of age, KO mice did not have their first estrous cycle until

approximately 90 days of age (Fig 3.4.1 A). This finding is consistent with the observation in chapter two that *Kiss1* and *Lrh-1* expression concurrently increased almost 2-fold after vaginal opening suggesting that LRH-1 may be important for promoting *Kiss1* expression during puberty.

After puberty, the time spent in each stage of the estrous cycle was monitored daily over a 6-8 week period. The female estrous cycle begins with diestrous, when serum FSH levels are low. FSH and estrogen levels rise throughout diestrous and peak in the late afternoon of proestrous, coinciding with completion of follicular maturation and the LH surge. Mice then ovulate and are fertile during estrous. KO mice spent 80-90% of the monitoring period in diestrous, while WT mice spent roughly 50% of the time in diestrous and cycled normally (Fig 3.4.1 B). The average number of cycles KO mice completed was significantly fewer than WT counterparts (Fig 3.4.1 C,D). A prolonged and inconsistent estrous cycle in mice can coincide with defects in fertility and reproductive capacity. Female KO mice were fertile, however, the time between litters was significantly higher in KO mice (Fig 3.4.1 E). WT mice consistently had a 25 day latency period between delivering litters, while KO mice had an average latency of 38 days between litters. This is consistent with KO mice rarely entering the fertile window of estrous.

Since KO animals cycled less often, but occasionally entered estrous, I hypothesized that pituitary FSH output was deleteriously affected by the loss of

kisspeptin tone in the arcuate nucleus. Serum analysis showed that in diestrous, KO mice had slightly lower serum FSH, and almost 2-fold lower serum FSH during estrous (Fig 3.4.1 F,G). Serum FSH was measured in *Lrh-1* Tg mice and WT littermates in diestrous, and was found to be almost 3-fold higher (Fig 3.4.1 H). Serum LH levels were unaffected by the KO in both diestrous and estrous (Fig 3.4.1 I,J). Serum estradiol also was unchanged in KO mice in diestrous (Fig 3.4.1 K). Interestingly, KO mice in estrous had significantly higher levels of serum estradiol (Fig 3.4.1 L). This was unexpected, considering that estrogen levels normally fall substantially during estrous in expectation of either pregnancy, or another estrous cycle. Serum FSH levels could not be reliably collected in KO mice in proestrous. WT mice consistently entered proestrous in the late afternoon prior to estrous, but, likely due to their disrupted estrous cycle pattern, KO mice could rarely be observed entering proestrous at this same time point.

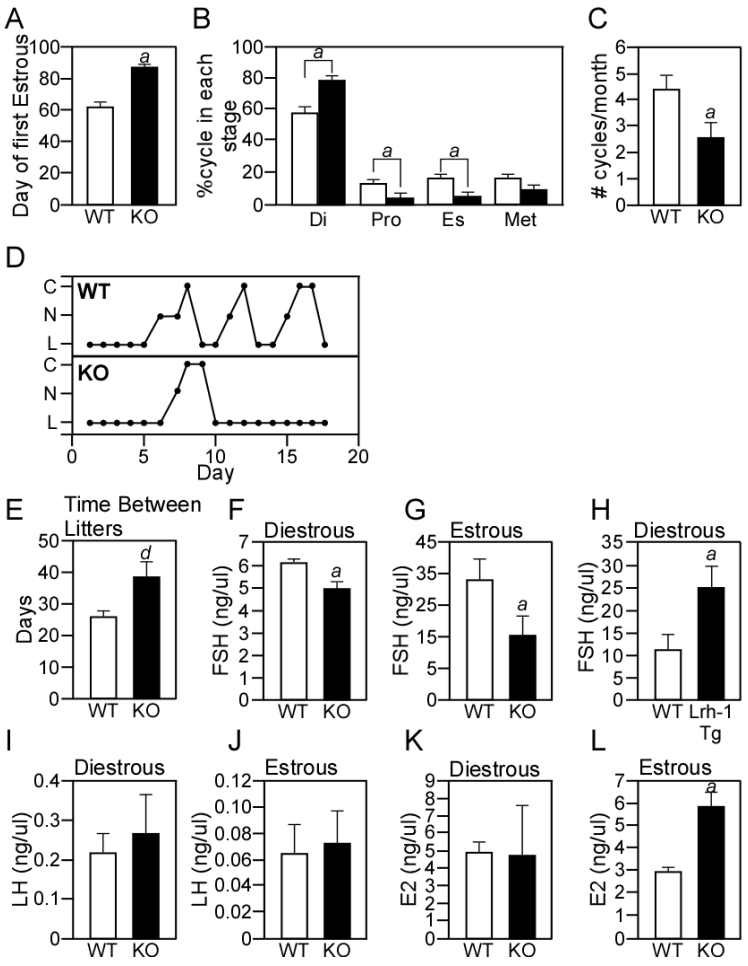

Fig 3.4.1 Deletion of *Lrh-1* from KISS1 neurons prolongs diestrous, reduces plasma FSH levels, and decreases fertility. A) Analysis of the day of first estrous during puberty in WT and KO mice (n=8 per group). B) Estrous cycle analysis, time spent in each stage of the estrous cycle was measured in WT and KO mice for 8 weeks (n=14 per group). Estrous stage was determined by microscopic analysis of cells collected from vaginal washes. C) Average number of times mice entered estrous in the 8 week period. D) 18 days of the estrous stage profile of a WT and KO mouse caged together during the 8 week period. E) Number of days between litters delivered by WT and KO mice (n=6 per group). F,G) Serum FSH levels of female WT and KO mice in diestrous, or estrous (n=5-8 per group). H) Serum FSH levels of female WT and *Lrh-1* Tg mice in diestrous (n=4 per group). I,J) Serum LH levels of female mice in either diestrous, or estrous (n=5-8 per group). K,L) Serum estradiol (E2) levels of female mice in either diestrous, or estrous. (n=5-8 per group). All of the above hormone measurements were done in the same animal cohorts in diestrous, or estrous. Error bars represent standard error of the mean. Letters above bars denote statistical significance values (student's T-test): *a*=<.05, *b*=<.01, *c*=<.005, *d*=<.001.

3.5 *Lrh-1* Deletion from Kiss1 Neurons Disrupts Ovarian Follicle Maturation

The low serum FSH, and high serum estradiol observed in KO mice during estrous, strongly suggested that reproductive timing defects might be partly driven by pathological ovarian follicle growth. Early stages of primary and secondary follicle maturation can proceed largely independent of FSH stimulus. Yet, later in the estrous cycle, when follicles mature into late secondary and larger graffian follicles, they require consistent FSH stimulus to continue maturation (Ryle 1973; Nelson, Felicio et al. 1982). I histologically examined ovaries from WT and KO mice in both diestrous, and estrous. In diestrous, KO ovaries appeared identical to those of WT mice (Fig 3.5.1 A,B). However, in estrous, KO ovaries contained a significantly higher number of follicles in all stages of the follicular maturation process (Fig 3.5.1 C,D). While KO mice in diestrous had no discernible difference in ovarian size or number of each follicle type (Fig 3.5.1 E), KO mice in estrous had significantly higher numbers of secondary and graffian follicles (Fig 3.5.1 F). This finding suggested that follicles beginning to mature during diestrous did not complete maturation and rupture in response to the LH surge. Consistent with this was the large number of fluid filled late antral follicular cysts still containing an oocyte observed in KO ovaries (Fig 3.5.1 G). KO ovaries had significantly fewer corpora lutea, the remnant of a successfully ruptured follicle (Fig 3.5.1 H). Ovaries from *Lrh-1* Tg mice contained few

oocytes, and larger corpora lutea like structures, suggesting that these follicles may be hyper-stimulated by the increased serum FSH levels (Fig 3.5.1 I,J).

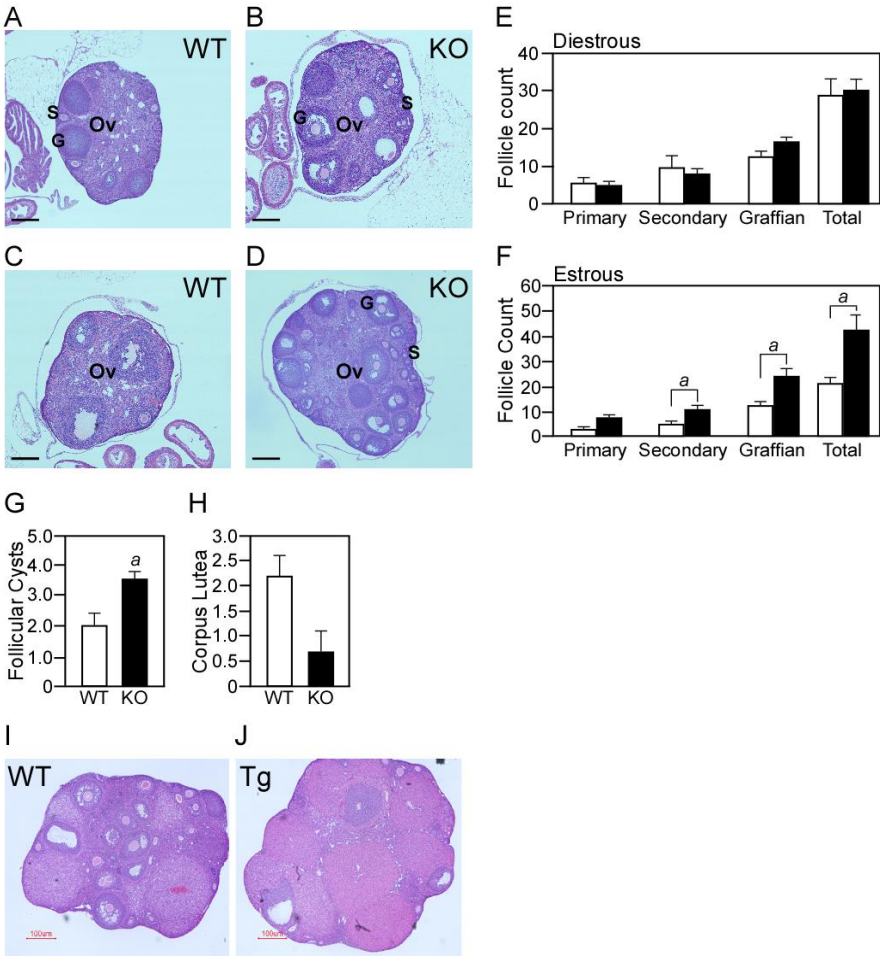

Fig 3.5.1 Ovaries of KO mice fail to complete follicular maturation and ovulate. A-D) 10x magnification of 25um sections of ovaries prepared by H&E from WT and KO mice in diestrous (A-B), or estrous (C-D) Scale bars: 100µm. Labels mark ovaries (Ov), secondary follicles (S), and graffian follicles (G). E) Analysis of follicle type number in diestrous (n=5-8). F) Analysis of follicle type number in estrous (n=5-8). G) Quantification of follicular cysts in ovaries. H) Quantification of the number of corpora lutea, an indicator of ovulation, in ovaries. I,J) Ovaries from WT or *Lrh-1* Tg mice in diestrous. Note the conspicuous lack of oocytes in (J) and large corpora lutea-like structures. (n=3). Error bars represent standard error of the mean. Letters above bars denote statistical significance values (student's T-test): *a*=<.05, *b*=<.01, *c*=<.005, *d*=<.001.

Steroidogenic acute Regulatory protein (*StAR*) and *Cyp17a*, two proteins whose expression is up-regulated in response to FSH stimulus, were significantly decreased in ovaries of KO mice (Fig 3.5.2 A,B). *Cyp19a1*, the rate-limiting enzyme in estrogen synthesis, was unchanged (Fig 3.5.2 C). Conversely, in KO mice that entered estrous, *StAR* levels returned to normal (Fig. 3.5.2 D). *Cyp17a* and *Cyp19a* expression were increased substantially in ovaries of KO mice in estrous, consistent with the higher serum estrogen levels in KO mice during estrous (Fig. 3.5.2 E,F).

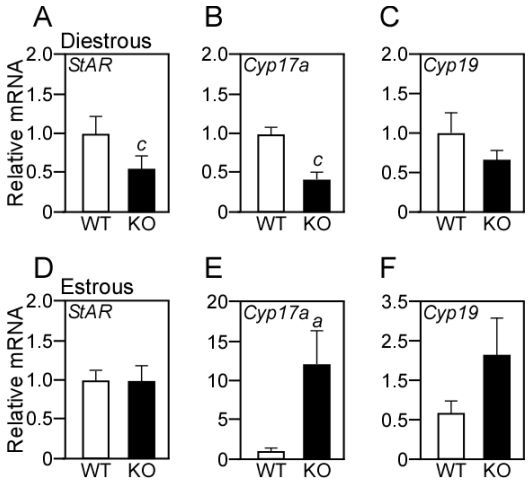

Fig 3.5.2 Ovaries of KO mice fail to correctly express steroidogenic enzymes. A-C) QPCR measurement of steroidogenic enzyme expression in ovaries from mice in diestrous (n=8). D-F) QPCR measurement of enzyme expression during estrous (n=5). Error bars represent standard error of the mean. Letters above bars denote statistical significance values (student's T-test): *a*=<.05, *b*=<.01, *c*=<.005, *d*=<.001.

3.6 Discussion

Previous studies showed that *Lrh-1* was expressed in the Arc of the hypothalamus in adult humans and mice. Here, I establish a role for LRH-1 in the Arc, where it is predominately expressed in KISS1 neurons, to directly control *Kiss1* expression in order to ensure proper FSH secretion from the pituitary and total reproductive function in females. Targeted deletion of *Lrh-1* from Arc KISS1 neurons causes a decrease in the basal tone of *Kiss1* expression. This presumably alters GnRH neuron output, causing a decrease in serum FSH levels. Conversely, targeted overexpression of *Lrh-1* in KISS1 neurons increases *Kiss1* expression and serum FSH levels. During follicular development, primary and secondary follicles first mature in an FSH-independent manner. They then reach a stage as graffian follicles in which they become dependent on FSH to finish maturation and prepare for ovulation in response to the LH surge. While WT FSH levels are normal and follicles complete maturation and ovulate, follicles in KO ovaries receive inadequate FSH stimulation, and are unable to mature. This results in many large, fluid filled oocyte-containing cysts, a decrease in ovulation, and a large refractory period between fertile windows. Interestingly, while more work needs to be done to completely understand the ovarian findings in the *Lrh-1* Tg mice, ovaries in these mice appear to be hyper-stimulated by the tonic increase in serum FSH, almost completely lacking in oocytes, and containing numerous

corpora lutea. These data suggest that LRH-1 function in the Arc is directly tied to follicular biology in the ovary.

LRH-1 works as a competence factor to stimulate a basal level of *Kiss1* expression in the Arc. This is likely responsible for sustaining a necessary level of *Kiss1* output by the Arc during diestrous. It has been observed in numerous studies that human patients with defects in energy balance due to obesity, anorexia, or other metabolic abnormalities, can experience diminished fertility. Many of these patients have decreased *Kiss1* levels, and their infertility can be rescued by KISS1 peptide injections. The mouse model developed demonstrates how a physiologic decrease in *Kiss1* levels in the Arc can result in disruptions in fertility, and strongly implies that small changes in the basal set point of KISS1 can significantly alter reproductive physiology.

References

d'Anglemont de Tassigny, X., L. A. Fagg, et al. (2007). "Hypogonadotropic hypogonadism in mice lacking a functional Kiss1 gene." Proc Natl Acad Sci U S A **104**(25): 10714-10719.

Fukuda, T., G. Scott, et al. (2006). "Generation of a mouse with conditionally activated signaling through the BMP receptor, ALK2." Genesis **44**(4): 159-167.

Han, S. K., M. L. Gottsch, et al. (2005). "Activation of gonadotropin-releasing hormone neurons by kisspeptin as a neuroendocrine switch for the onset of puberty." J Neurosci **25**(49): 11349-11356.

Kotani, M., M. Detheux, et al. (2001). "The metastasis suppressor gene KiSS-1 encodes kisspeptins, the natural ligands of the orphan G protein-coupled receptor GPR54." J Biol Chem **276**(37): 34631-34636.

Lee, Y. K., D. R. Schmidt, et al. (2008). "Liver receptor homolog-1 regulates bile acid homeostasis but is not essential for feedback regulation of bile acid synthesis." Mol Endocrinol **22**(6): 1345-1356.

Mayer, C., M. Acosta-Martinez, et al. (2010). "Timing and completion of puberty in female mice depend on estrogen receptor alpha-signaling in kisspeptin neurons." Proc Natl Acad Sci U S A **107**(52): 22693-22698.

Mayer, C. and U. Boehm (2011). "Female reproductive maturation in the absence of kisspeptin/GPR54 signaling." Nat Neurosci **14**(6): 704-710.

Messager, S., E. E. Chatzidaki, et al. (2005). "Kisspeptin directly stimulates gonadotropin-releasing hormone release via G protein-coupled receptor 54." Proc Natl Acad Sci U S A **102**(5): 1761-1766.

Mueller, J. K., A. Dietzel, et al. (2011). "Transcriptional regulation of the human KiSS1 gene." Mol Cell Endocrinol **342**(1-2): 8-19.

Nelson, J. F., L. S. Felicio, et al. (1982). "A longitudinal study of estrous cyclicity in aging C57BL/6J mice: I. Cycle frequency, length and vaginal cytology." Biol Reprod **27**(2): 327-339.

Ryle, M. (1973). "Gonadotropins and ovarian function." Acta Eur Fertil **4**(3): 113-122.

Topaloglu, A. K., J. A. Tello, et al. (2012). "Inactivating KISS1 mutation and hypogonadotropic hypogonadism." N Engl J Med **366**(7): 629-635.

CHAPTER FOUR

Kiss1 is an LRH-1 Target Gene

4.1 Introduction

Kiss1 expression in the arcuate nucleus (Arc) was decreased in the KISS1 specific *Lrh-1* knockout mouse. Likewise, over-expression of *Lrh-1* in KISS1 neurons of transgenic mice caused a concomitant increase in *Kiss1* expression. These data suggested that *Kiss1* might be an LRH-1 target gene. LRH-1 most often functions to set a basal tone of transcription of its target genes. While many target genes for LRH-1 are known in the enterohepatic system, pancreas, and ovary; few are known elsewhere in the body, and none are known for LRH-1 in the brain.

The *Kiss1* gene is located on chromosome 1 in rodents and humans. It is 2,511 basepairs (bp) long in rodents. The transcribed region consists of a small 5'cap, an 81bp exon 1, a large intron, a second exon, and the 3'polyA tail. The processed length of the mRNA is 381bp, and the protein product is 126 amino acids. The human *Kiss1* gene differs considerably, in that it consists of four exons, although the first intronic region is still the longest (Mueller, Dietzel et al. 2011). Studies have suggested that the *Kiss1* promoter comprises at least 3000bp of the region upstream of the transcriptional start site (TSS) (Gottsch, Navarro et al. 2009). ERα binds in a non-classical manner (meaning it does not directly bind

DNA as a homodimer) to a region 2000bp upstream of the TSS. There is evidence that AP-1, GATA-2, and other transcription factors activate the *Kiss1* promoter (Mueller, Dietzel et al. 2011). Interestingly, LRH-1 is known to associate with GATA-2 on the promoter of LHβ in pituitary cells to potentiate gonadotropin subunit expression.

This chapter describes the experiments used to test the hypothesis that *Kiss1* is an LRH-1 target gene. Chromatin immunoprecipitation of LRH-1 on the *Kiss1* promoter showed that LRH-1 bound to two distinct regions of the promoter. Roughly 4-kilobases (kb) of the mouse *Kiss1* promoter was cloned and constructs were created to determine which LRH-1 response element was important for promoter activation. From these data, LRH-1 appears to bind to a site 228bp downstream of the TSS, in the first intron, to activate the promoter. This site is conserved in mouse, rat, and can be found in intron 1 of the human *Kiss1* gene. *Kiss1* is the first target gene of LRH-1 in the adult brain.

4.2 Lrh-1 Binding Sites by Chromatin Immunoprecipitation

I tested whether LRH-1 could directly bind to the *Kiss1* gene promoter using chromatin immunoprecipitation (ChIP). Working with Jamie Boney-Montoya and Serkan Kir in the Mangelsdorf Lab I developed ChIP protocols for use in the Arc. This is a difficult target due to its high lipid content and low nucleus number. I succeeded by pooling two arcuate nuclei per chromatin sample,

by using buffers suitable for chromatin extraction from neurons, and by using a bath sonicator instead of a probe sonicator to minimize sample loss during sonication. Later, I was able to maximize chromatin stability during preparation and optimize the use of magnetic beads for immunoprecipitation, and was able to then use only one arcuate nucleus per sample and get extremely low background levels.

ChIP was performed on whole Arc samples dissected from female WT mouse brains in diestrous. A previously validated ChIP-grade LRH-1 antibody was used for immunoprecipitation. Normal IgG antibodies were used as negative controls and did not enrich for any areas of the *Kiss1* gene promoter in any of these experiments. Fold enrichment over input was determined using QPCR and primer pairs specific for regions spaced every 500-1000bp upstream and downstream of the transcription start site (TSS). ChIP results showed that LRH-1 bound to the *Kiss1* promoter at two regions, one -3700bp upstream of the TSS (-3700 region), and another +228bp downstream of the TSS located in the first intron of the *Kiss1* gene (+228 region) (Fig 4.2.1 A). There was no binding to control regions 4100bp upstream, or 400bp downstream of the TSS. A region -1000bp upstream of the TSS in the middle of the promoter was never bound by LRH-1. Interestingly, ChIP for ERα (Fig 4.2.1 B), and for acetylation of histone 3 (Acetyl-H3, Fig 4.2.1 C) showed the same pattern of enrichment. A diagram of these regions within the *Kiss1* promoter can be seen in Fig 4.2.1 D. This

suggested that LRH-1 bound to regions of the promoter that were possibly important for ERα function or overall transcriptional activation.

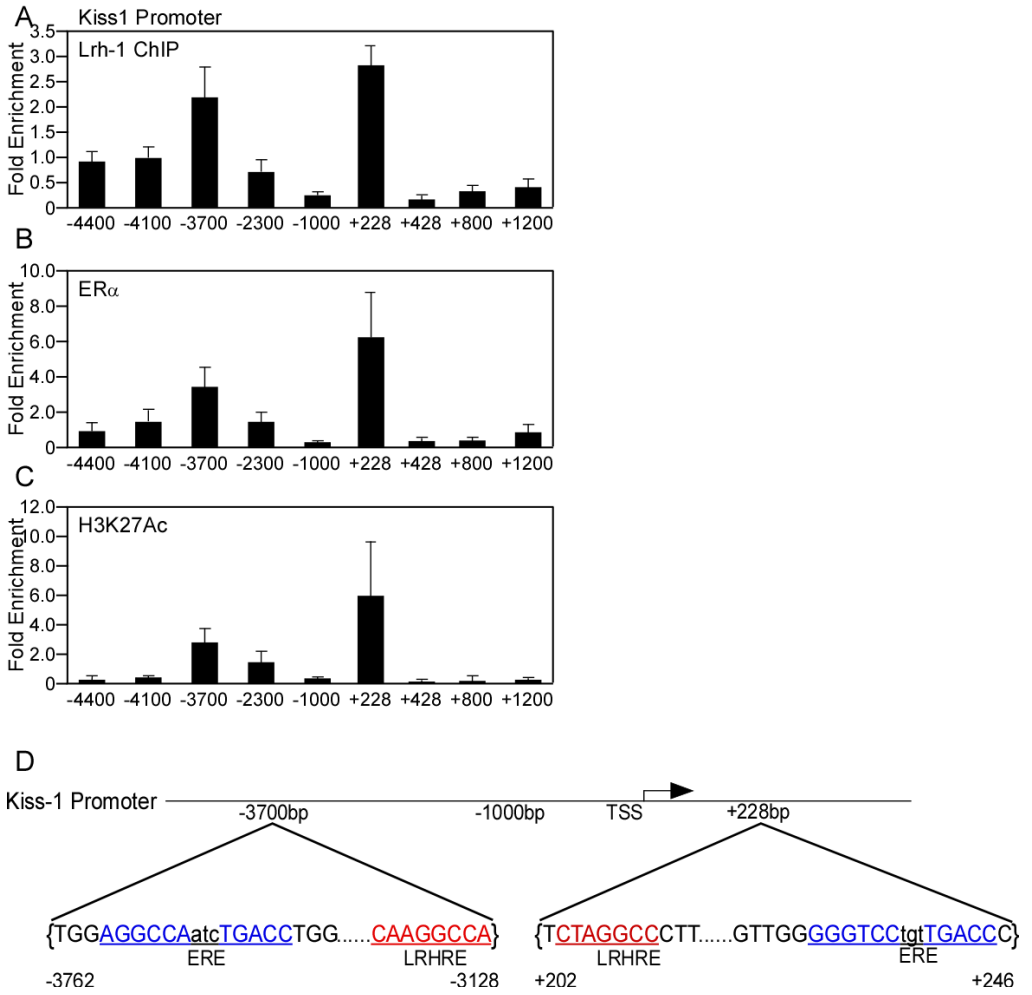

Fig 4.2.1 Chromatin Immunoprecipitation for LRH-1, ERα, and H3K27Ac on the *Kiss1* promoter. A) ChIP using a monoclonal LRH-1 antibody in freshly dissected Arc tissue. Primers span 4500bp upstream, and 1200bp downstream of the TSS). B) ChIP for ERα as a positive control using a previously published antibody. C) H3K27Ac ChIP, demonstrating transcriptionally active motifs along the *Kiss1* promoter. D) Schematic of the *Kiss1* promoter and the putative LRH-1 binding sites (LRHRE, red, underlined) and ERα binding sites (ERE, blue, underlined) and their locations relative to the TSS. These ChIP data are representative of three separate ChIP experiments on different animal cohorts giving identical results. Error bars represent standard error of the mean.

4.3 LRH-1 Activates the Kiss1 Promoter In Vitro

ChIP data suggested that LRH-1 bound directly to specific regions of the *Kiss1* promoter *in vivo.* To explore the functional significance of LRH-1 binding to the *Kiss1* promoter, and determine which binding site may be most important for transcriptional control of *Kiss1*, I utilized an *in vitro* cell culture luciferase-based reporter assay. 4kb of the mouse *Kiss1* promoter was cloned, and from this, differing lengths of the *Kiss1* promoter were sub-cloned into a pGL4-luc2 vector backbone. I first made three different luciferase reporter constructs containing differing lengths of the *Kiss1* promoter (Fig 4.3.1 A). The first, considered "full-length" (named pKiss) contained a promoter fragment beginning upstream of the -3700bp region, and ending after the +228 region found in ChIP experiments. The second construct was identical to pKiss, but excluded the -3700bp region of the *Kiss1* promoter (pKiss-*3700*). The third construct consisted of only the *Kiss1* TSS, and the +228 site (pKiss+*228*).

Promoter constructs were co-transfected either with or without an *Lrh-1* expression vector. A β-galactocidase expression vector was used as a transfection efficiency control. A luciferase construct containing the human *SHP* promoter LRH-1 response element was used as a positive control for LRH-1 activity and gave approximately 4-fold activation under our conditions (Fig 4.3.1 B). LRH-1 increased kisspeptin promoter activity by more than 2-fold from the pKiss vector (Fig 4.3.1 C). The truncation vectors pKiss-*3700, and pKiss+228* showed

identical activity to the full-length pKiss. These data suggested that while LRH-1 bound to two regions of the promoter in our ChIP experiments, the primary LRHRE was likely confined to the +228bp region. Interestingly, a luciferase-reporter vector analogous to pKiss but completely lacking the +228bp region, lost significant basal activity in the transient transfection assays, suggesting that this region may be important for binding of other positive transcription factors as Ill (Fig 4.3.1 D).

In a separate set of experiments, 300bp regions of the Kiss1 promoter consisting of the sites analyzed in ChIP experiments were sub-cloned into a TK-luciferase vector backbone. This vector differs from pGL4-luc2 in that it contains a minimal TK promoter which helps drive expression when only small fragments of DNA are inserted. These three constructs were named pTK3700, pTK1000, and pTK228 respectively (Fig. 4.3.1 E). These were co-transfected with LRH-1 to test if the -3700bp and +228bp LRHRE had specific activity outside of the *Kiss1* promoter environment. Surprisingly, luciferase expression of pTK3700 was repressed by the presence of Lrh-1 (Fig. 4.3.1 F). LRH-1 had no effect on the activity of pTK1000 (Fig. 4.3.1 G), consistent with the lack of LRH-1 binding in ChiP. LRH-1 significantly activated the pTK228 vector (Fig. 4.3.1 H). This independently verified the ability of this region in the *Kiss1* promoter to be activated by LRH-1. Taken together, these data suggest that the +228bp site in the *Kiss1* promoter is the dominant site for control of expression by LRH-1.

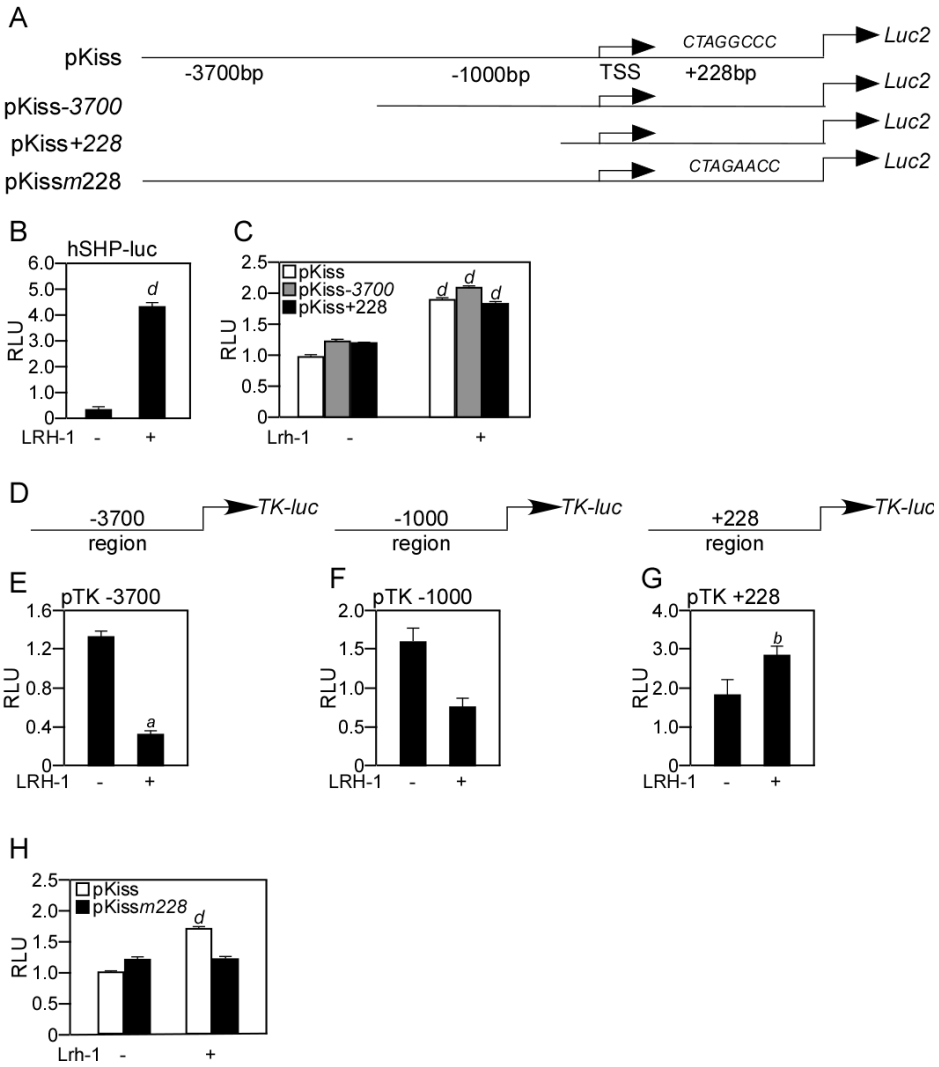

Fig 4.3.1 LRH-1 activates the *Kiss1* promoter *in vitro.* A) Schematic of the cloned mouse *Kiss1* promoter, and the constructed luciferase expression vectors used in (C). B) Transient transfection assay of LRH-1 and a positive control vector containing the LRHRE in human SHP promoter. C) The first three *Kiss1* promoter luciferase vectors in (A) co-transfected either without, or with an LRH-1 expression vector. D) Three 300bp regions of the *Kiss1* promoter were cloned into a TK-luc expression vector. E-G) co-transfection assays of the vectors either with, or without Lrh-1. H) Transient transfection assay of pKiss, and mutated pKissm228 vectors with or without an LRH-1 expression vector. LRH-1 loses all activity upon mutation of the +228 region. Error bars represent standard error of the mean. Letters above bars denote statistical significance values (student's T-test): *a*=<.05, *b*=<.01, *c*=<.005, *d*=<.001.

Computational inspection of the +228bp region did not reveal a perfectly conserved LRHRE consensus sequence (CAAGGcc). However, a nearly homologous putative LRHRE was found with the sequence CTAGGccC at site +204bp. To test if this site was responsible for the induction of *Kiss1* promoter activity *in vitro,* I created a fourth luciferase-reporter construct (Fig 4.3.3 A, pKissm228). This construct was identical to pKiss, but the putative LRHRE in the +228bp region was mutated to CTAGAACC to disrupt possible LRH-1 binding.

Transient co-transfection experiments comparing the activity of pKiss, to pKissm228, were performed with or without the inclusion of an LRH-1 expression vector. As previously, LRH-1 caused a consistent 2-fold activation of the pKiss vector. However, the pKiss*m228* vector, with two base pair mutations in the putative LRHRE, could not be activated by LRH-1 (Fig 4.3.3 B). These data, taken together with KO, *Lrh-1* Tg, and ChIP experimental findings, suggest that LRH-1 directly binds and activates the *Kiss1* promoter. It does so by using a putative LRHRE +228bp downstream of the TSS, setting a basal level of *Kiss1* expression in the Arc, and consequently regulating and maintaining the tone of FSH secretion needed during follicular maturation.

4.4 Discussion

These experiments were implemented to determine if LRH-1 directly controlled *Kiss1* expression, and offered a mechanism to explain how the loss or gain of LRH-1 function in our animal models causes the reproductive phenotypes. ChIP experiments showed that LRH-1 directly bound to two regions of the *Kiss1* promoter *in vivo*. Cell culture experiments demonstrated that LRH-1 can activate the *Kiss1* promoter, and demonstrated that the LRH-1 transactivation activity was confined to a region +228bp downstream of the TSS. This site did not contain a perfectly conserved LRHRE, but did contain one closely matching in sequence, which upon mutation lost all LRH-1 activation potential. In terms of the lack of perfect conservation to the ideal LRHRE sequence, it is important to note that KO of *Lrh-1* caused only a two-fold decrease in *Kiss1* expression, and there was almost a 1:1 ratio of *Lrh-1* to *Kiss1* over-expression in the *Lrh-1* Tg mouse model. Similarly, *in vitro,* LRH-1 only stimulated the *Kiss1* promoter by 2-fold. These data suggest that while LRH-1 is important for *Kiss1* biology, *Kiss1* expression may be modulated by other transcription factors that may be inhibiting any further induction. Likely, this is precisely due to the lack of perfect sequence conservation in the LRHRE we discovered.

Besides the biological findings, it is important to note that the knockout and transgenic mice generated in this study are novel models for a number of reasons. There are currently very few mouse lines in which the KISS1 neurons are

targeted directly. In two mouse lines, *Kiss1* expression was abrogated from the neurons, and another expressed diphtheria toxin in the neurons to lead to their cytotoxic ablation (d'Anglemont de Tassigny, Fagg et al. 2007; Lapatto, Pallais et al. 2007; Mayer and Boehm 2011). The only mouse line targeting the deletion of a protein other than Kiss1 was an infertility model that deleted ERα from KISS1 neurons (Mayer, Acosta-Martinez et al. 2010). Beyond that work, no studies have used *in vivo* mouse models to examine the role of other proteins or transcription factors in regulating *Kiss1* expression. Importantly, all previous studies on the control of *Kiss1* expression by specific transcription factors other than ERα have been done *in vitro*. Also, this study comprises the first work using chromatin immunoprecipitation of the *Kiss1* promoter *in vivo*, and extending that work to examining the promoter *in vitro.* Hopefully, through publication of this work, other labs will begin to use these techniques to more rigorously study the control of *Kiss1* expression in the hypothalamus.

This study gives compelling evidence for a nuclear receptor based transcriptional circuit in which LRH-1 sets a basal tone of *Kiss1* expression in the Arc, independent of the repressive effects of ERα. The absence of LRH-1 from AVPV KISS1 neurons offers a mechanism of how KISS1 neurons, spatially segregated into two regions of the hypothalamus, work to control fertility by maintaining different aspects of pituitary output (Fig 4.4.1). The basal stimulation of *Kiss1* expression by LRH-1 is needed to sustain the increasing concentrations

of pituitary FSH output that follicles need for maturation. Once follicles are mature and plasma estrogen levels peak, estrogen-bound ERα represses Arc *Kiss1* expression. This likely causes the drop in serum FSH after estrous. In turn, AVPV *Kiss1* expression, which is not basally set by LRH-1, can be maximally increased by ERα stimulation to cause the LH surge needed for ovulation. Thus, the presence of LRH-1 in the Arc allows for constant maintenance of the output of FSH, while the lack of LRH-1 in the AVPV, allows for a more transient burst of activity needed to surge the output of LH.

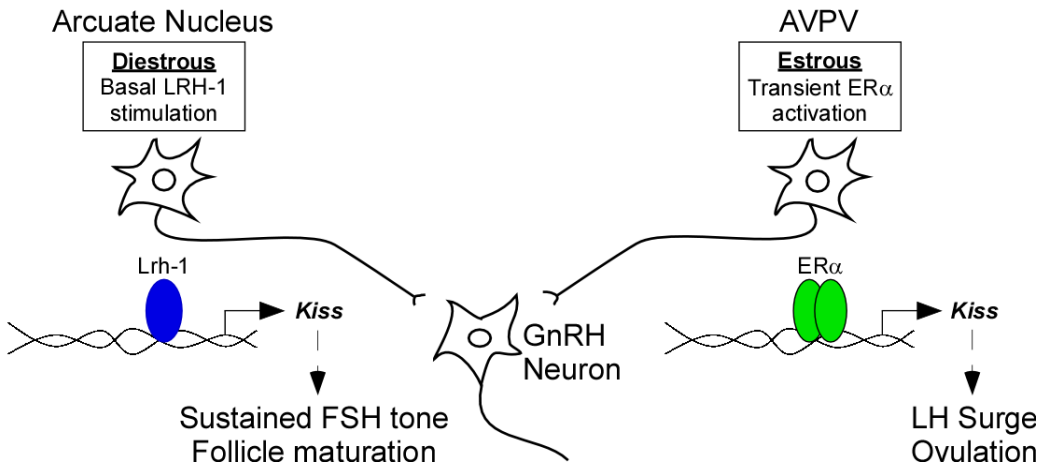

Fig 4.4.1 LRH-1 sets the basal tone of *Kiss1* expression in the Arc to maintain FSH output and ensure follicular maturation. The basal stimulation of *Kiss1* expression by LRH-1 sustains FSH output by the pituitary during diestrous. This is important for sustaining pituitary gonadotropin output and follicular maturation. At proestrous, this is subject to the ERα mediated repression of Arc *Kiss1* expression. Simultaneously, in proestrous, ERα stimulates KISS1 neurons in the AVPV to elicit a burst of *Kiss1* expression and the subsequent LH surge. The absence of LRH-1 from AVPV KISS1 neurons likely minimizes basal AVPV *Kiss1* output to allow large bursts of activity to occur.

A major function of LRH-1 is its coordination of activity across multiple tissues related by a common metabolic function. In the ovary, LRH-1 works with ERα to regulate transcription of Cyp19a and progesterone synthesis enzymes needed for steroid hormone production. In the pituitary LRH-1 is important for gonadotropin subunit expression. Now, I show that LRH-1 is functioning in the Arc to ensure the pituitary receives the stimulus necessary to express and secrete pituitary gonadotropins. The function of LRH-1, from the ovary to the arcuate and back, is vital for proper function of the entire reproductive axis.

References

d'Anglemont de Tassigny, X., L. A. Fagg, et al. (2007). "Hypogonadotropic hypogonadism in mice lacking a functional Kiss1 gene." Proc Natl Acad Sci U S A **104**(25): 10714-10719.

Gottsch, M. L., V. M. Navarro, et al. (2009). "Regulation of Kiss1 and dynorphin gene expression in the murine brain by classical and nonclassical estrogen receptor pathways." J Neurosci **29**(29): 9390-9395.

Lapatto, R., J. C. Pallais, et al. (2007). "Kiss1-/- mice exhibit more variable hypogonadism than Gpr54-/- mice." Endocrinology **148**(10): 4927-4936.

Mayer, C., M. Acosta-Martinez, et al. (2010). "Timing and completion of puberty in female mice depend on estrogen receptor alpha-signaling in kisspeptin neurons." Proc Natl Acad Sci U S A **107**(52): 22693-22698.

Mayer, C. and U. Boehm (2011). "Female reproductive maturation in the absence of kisspeptin/GPR54 signaling." Nat Neurosci **14**(6): 704-710.

Mueller, J. K., A. Dietzel, et al. (2011). "Transcriptional regulation of the human KiSS1 gene." Mol Cell Endocrinol **342**(1-2): 8-19.

CHAPTER FIVE

The Role of LRH-1 in POMC Neurons

5.1 Introduction

Profiling of LRH-1 in the arcuate nucleus (Arc) showed that it was expressed in approximately 20% of POMC neurons. This was a small subset of POMC neurons, but still deserved study. POMC neurons are involved in the control of food intake and energy expenditure. As outlined in the introduction of this dissertation, upon food intake, increased serum leptin causes POMC neurons to activate autonomic pathways that bring about the cessation of food intake and the modulation of energy expenditure and serum glucose. POMC neurons coordinate autonomic nervous system output with energy status by responding to hormones, such as leptin, released by the adipose and gut (Elmquist, Elias et al. 1999; Zigman, Jones et al. 2006; Dampney 2011). POMC neurons express a number of cell surface receptors, which they mediate hormone activation. Among the POMC population there is a non-heterogeneous expression pattern of the leptin receptor, ghrelin receptor, and others. This non-heterogeneity is important for their ability to respond and integrate information from multiple peripheral hormones (Williams, Margatho et al. 2010). LRH-1 expression was non-heterogeneous as well, and therefore might be important in POMC neuron biology.

To study the role of LRH-1 in POMC neurons I constructed a POMC specific Lrh-1 knockout mouse line. The POMC-Cre line was graciously donated from the Dr. Joel Elmquist lab. This mouse line, and the data in this chapter, was actually the first project I accomplished in elucidating the role of LRH-1 in the Arc. A year later the KISS1-cre mouse line was constructed by the Dr. Carol Elias lab, and became the primary focus of effort in my dissertation.

This chapter details the evidence that LRH-1 may not play a role in POMC neuron biology. POMC specific LRH-1 knockout mice (pKO mice) had a metabolic phenotype specific only to females. Female pKO mice gained less weight than WT littermates after 8 weeks on a high fat high calorie western diet. Body composition analysis showed that on this diet they had higher fat mass, and lower lean mass than WT mice. Metabolic cage analysis showed that oxygen consumption in pKO mice was higher than in WT littermates. Unfortunately, it was not possible to elucidate any potential target genes of LRH-1 in POMC neurons, nor identify a role for LRH-1 in these neurons, that could offer a mechanism behind these phenotypes. The mechanism of action of LRH-1 in the Arc that could explain these phenotypes is still unknown.

5.2 Generation of a POMC Specific LRH-1 Knockout Mouse

A POMC-Cre mouse line was crossed with the *Lrh-1*$^{lox/lox}$ line. The resulting POMC specific *Lrh-1* knockout mouse is referred to here as “pKO”

mouse. Laser capture microdissection was used to collect Arc tissue from pKO and WT mice. QPCR of the captured Arc demonstrated that *Lrh-1* expression was significantly decreased (Fig 5.2.1 A). *Cre* expression was significantly higher in pKO Arc (Fig 5.2.1 B) No decrease in *Lrh-1* expression was seen in peripheral tissues examined, though a small but insignificant decrease was seen in colon and ovaries of pKO mice (Fig 5.2.1 C,D). *Lrh-1* levels were unchanged in the pituitary (Fig 5.2.1 E).

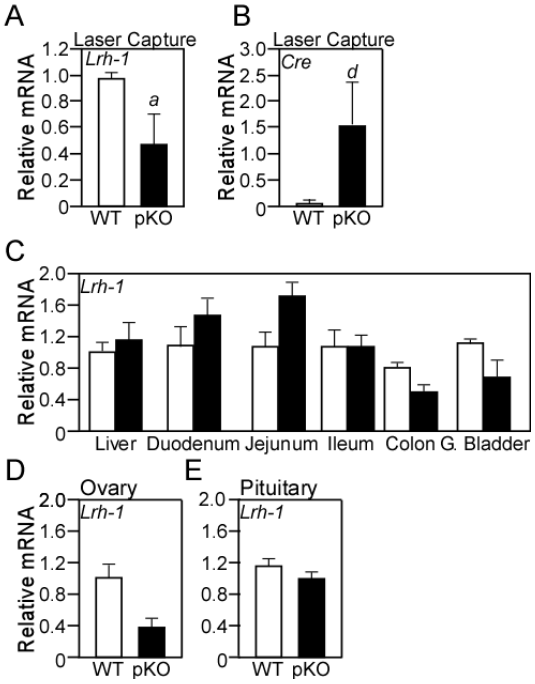

Fig 5.2.1 POMC specific LRH-1 knockout mouse (pKO) creation. A) Laser capture microdissection (LCM) Arc samples were assayed via QPCR (n=3). *Lrh-1* expression was decreased in the LCM samples of pKO mice. B) *Cre* expression was significantly increased in the same LCM samples. C) *Lrh-1* expression was unchanged in peripheral tissues of pKO mice (n=6). D,E) Ovary and pituitary levels of *Lrh-1* expression were unchanged (n=6). Error bars represent standard error of the mean. Letters above bars denote statistical significance values (student's T-test): *a*=<.05, *b*=<.01, *c*=<.005, *d*=<.001.

Since LRH-1 is involved in stem cell pluripotency, I examined whether a brain specific knockout would cause any developmental defects in brain parenchyma morphology. Brains of pKO mice were examined by immunohistochemistry to label POMC neurons, and by nissl staining to investigate whether *Lrh-1* knockdown had caused any morphological changes to POMC neuron number or the size and shape of the Arc. No differences were seen in POMC neuron number (Fig 5.2.2 A,B,E). Similarly, Arc morphology was normal in the pKO mouse (Fig 5.2.2 C,D).

After the phenotypes of this mouse line were discovered (discussed below), I attempted to identify putative LRH-1 target genes in POMC neurons, the expression levels of a large number of genes were checked by QPCR in the Arc of the pKO mouse line. *Pomc* and *Npy* expression were unchanged in the Arc of these animals (Fig 5.2.2 F,G) As well, no differences were seen in fatty acid synthase (FAS), leptin receptor (LepR), ghrelin receptor (Ghsr), the membrane bound glucose transporter 4 (Glut4), melanocortin 4 receptor (Mc4R), or suppressor of cytokine signaling 3 (Socs3). Unfortunately, I was never able to identify an LRH-1 target gene in POMC neurons, nor demonstrate any molecular link between LRH-1 activity in the Arc, and the pKO mouse phenotypes discussed below.

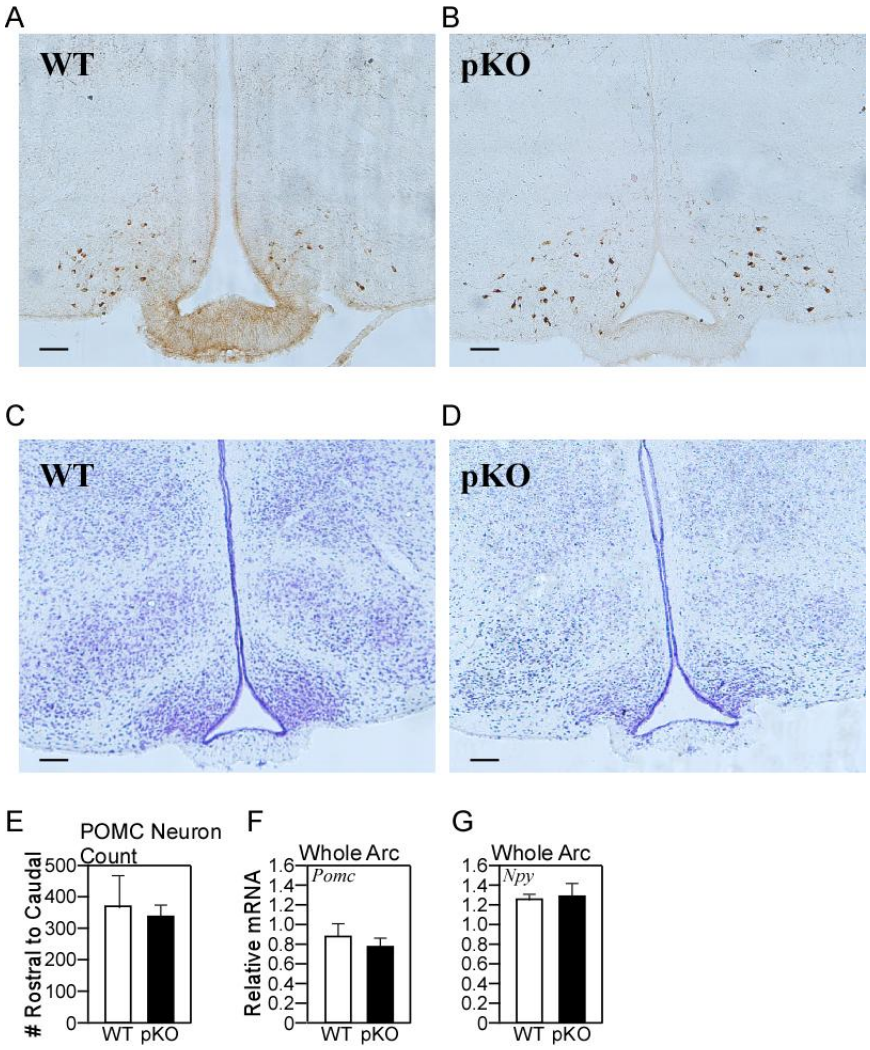

Fig 5.2.2 POMC neuron number and Arc morphology are unchanged in pKO mice. A,B) β-endorphin immunohistochemistry labeling POMC neurons in male brain tissue from WT and pKO mice (10x magnification, bright field microscopy, scale bars: 100μm, n=3 mice per group). C,D) Nissl stain of brain tissue from male WT and pKO mice (n=3). E) Quantification of Pomc neuron number in (A,B). Labeled POMC neurons were counted throughout the complete rostral to caudal length of the Arc. F) *Pomc* neuropeptide expression in dissected whole Arc (n=5-6 per group). G) *Npy* neuropeptide expression in the same samples. Error bars represent standard error of the mean. Letters above bars denote statistical significance values (student's T-test): *a*=<.05, *b*=<.01, *c*=<.005, *d*=<.001.

5.3 pKO Mice are Phenotypically Normal on a Chow Diet

Since POMC neurons are involved in controlling food intake and energy expenditure, I first asked if this mouse line had any basal defects in these functions. Littermate WT and pKO mice were individually caged and fed a chow diet. Body weight and food intake were tracked for 6 weeks. No differences were seen in starting body weight, rate of body weight increase, or food intake of male and female pKO mice on the chow diet (Fig 5.3.1 A-C). After a 24-hour fast, pKO mice responded by eating the same amount of food as WT mice (Fig 5.3.1 D). POMC neurons are known to respond to serum glucose levels and possibly regulate endocrine pancreas function. Fasted levels of serum insulin and glucose were measured, showing no differences between pKO and WT mice (Fig 5.3.1 E,F). These results suggested that, at baseline, pKO mice have no appreciable difference in autonomic nervous system behavior.

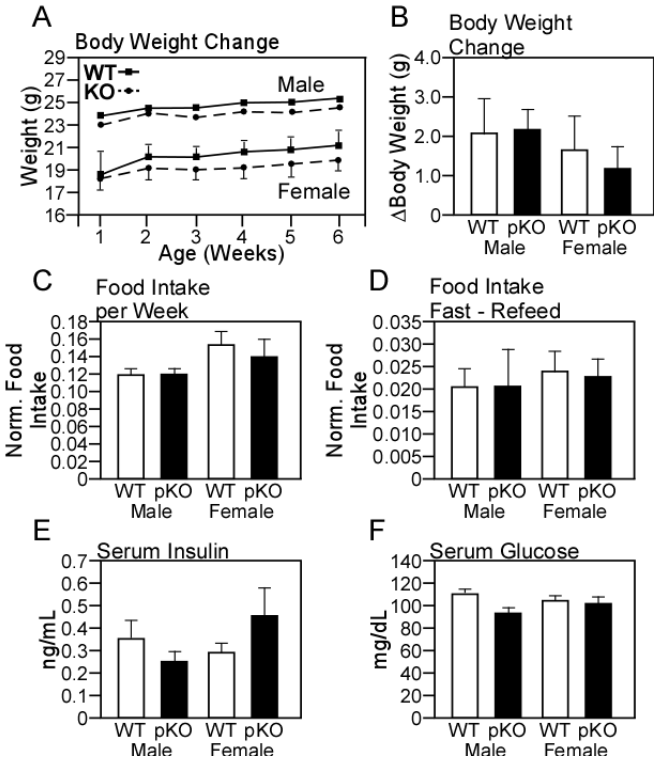

Fig 5.3.1 pKO mice have normal weight gain and food intake on a chow diet. A) Body weight gain in male and female WT and pKO mice on a chow diet. B) Final changes in body weight from (A). C) Normalized food intake per week in WT and pKO mice of both genders. Food intake was normalized to number of days between measurements and weight of each mouse. D) Food intake after a 24 hour fast – refeed challenge. E) Serum insulin levels in mice after an overnight fast. F) Serum glucose levels in mice after an overnight fast. N=8 animals per group all experiments performed on the same cohort of animals. Error bars represent standard error of the mean. Letters above bars denote statistical significance values (student's T-test): *a*=<.05, *b*=<.01, *c*=<.005, *d*=<.001.

5.4 Female pKO Mice Gain Less Weight on a Western Diet

Many mouse models do not demonstrate a significant phenotype until put under some form of metabolic or physiological stress. I decided to metabolically challenge the pKO mice by putting them on a high fat calorie, high cholesterol "western diet". Male and female pKO mice and WT littermates were placed on the western diet for 8 weeks. Body weight and food intake were monitored weekly, and insulin and glucose measurements were taken at the end of the study. Male pKO mice in the study exhibited no differences in any of these parameters from their WT counterparts (Fig 5.4.1 A-C). Interestingly, female pKO mice gained significantly less weight than WT mice (Fig. 5.4.1 A). However, this difference was slight, and only statistically significant in the 8^{th} week time point. Food intake was slightly higher in females, but this was not significant (Fig. 5.4.1 C). No differences were found in serum insulin or glucose levels between the groups (Fig. 5.4.1 D,E). These findings suggested that female pKO mice may be slightly less susceptible to weight gain on a western diet, which is a phenotype often consistent with changes in autonomic governance of energy status.

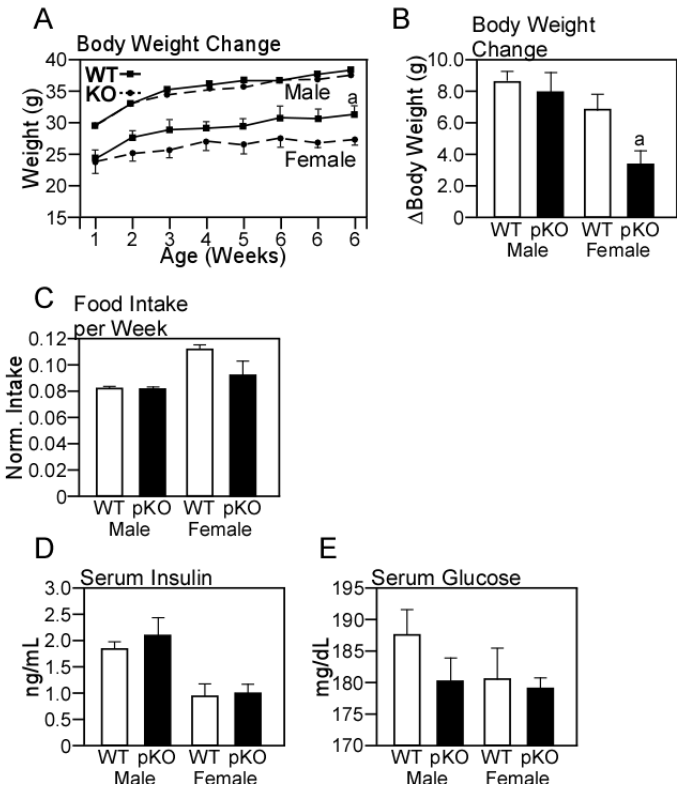

Fig 5.4.1 Female pKO mice are resistant to weight gain on a western diet. A) Body weight gain in male and female WT and pKO mice on a western diet. B) Final changes in body weight from (A). C) Normalized food intake per week in WT and pKO mice of both genders. Food intake was normalized to number of days between measurements and weight of each mouse. D) Serum insulin levels in mice after an overnight fast. E) Serum glucose levels in mice after an overnight fast. N=10 animals per group all experiments performed on the same cohort of animals. Error bars represent standard error of the mean. Letters above bars denote statistical significance values (student's T-test): *a*=<.05, *b*=<.01, *c*=<.005, *d*=<.001.

An increased basal metabolic rate will increase energy burning in the animal and can protect the animal from weight gain (Parton, Ye et al. 2007). To test whether female pKO mice have any differences in metabolic rate, I placed female WT and pKO mice, either on a chow diet or a western diet, in metabolic cages. Metabolic activity was calculated by measuring the animal's O_2

consumption, heat production, and amount of CO_2 expired. Female pKO mice had increased O_2 consumption, heat production, and CO_2 expiration. Food and water intake were unchanged between groups. Surprisingly, this increased energy state occurred while on the chow diet, and not while on the western diet (Fig. 5.4.2 A-C). This result was unexpected, considering that female animals had decreased weight gain on a western diet, and were phenotypically normal on a chow diet.

MRI analysis of body composition was conducted in these animals and demonstrated that female pKO mice had higher body fat, and less lean mass than WT littermates (Fig. 5.4.2 D-F). This finding was also largely not in-line with what I would expect in an animal with a higher metabolic rate, as they should have lower fat mass and higher lean mass. The conflicting results caused me to largely question the actual fidelity of the mouse line. I repeated the western diet experiment and metabolic cage experiment on other cohorts of mice and could not replicate the initial findings. In fact, sometimes the results would be opposite of the previous findings. MRI data were also inconsistent between cohorts of litter-matched mice. Due to this high level of inconsistency between litters, and the absence of any gene changes in the Arc to mechanistically validate these findings, I discontinued the project on grounds that the mouse line was presenting with inconsistent and irreconcilable phenotypes. Taken together, the pKO mouse line had a fairly subtle phenotype which could not be repeated and that could not be

linked with measurements of metabolic activity or POMC neuron gene expression activity.

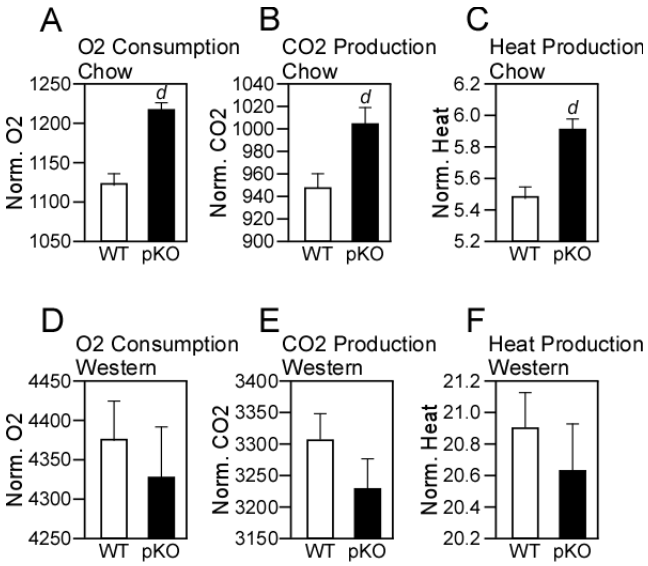

Fig 5.4.2 Female pKO mice have increased energy expenditure on a chow diet, but not a western diet. A) O2 consumption in metabolic cages of WT and pKO mice on a chow diet. B) CO2 consumption o the same cohorts. C) Heat production, as measured by cage temperature, in the same experiment. D-F) A separate age-matched cohort of mice on a western diet were placed in metabolic cages to measure the same parameters. Both experiments were performed identically. N=6 animals per group in all experiments performed. Error bars represent standard error of the mean. Letters above bars denote statistical significance values (student's T-test): *a*=<.05, *b*=<.01, *c*=<.005, *d*=<.001.

5.5 Discussion

These studies demonstrated the lack of a known role for LRH-1 in POMC neurons. While the female mice did have a subtle resistance to weight gain on a western diet, this result could not be corroborated by metabolic cage data. More importantly, metabolic cage data and body composition analysis gave conflicting

results and were ultimately contradictory to the resistance to weight gain. Taken together, this made me seriously doubt the possibility that there would be a direct, causal link between these phenotypes and LRH-1 activity in the Arc. Laser capture microdissection and conventional dissection of the Arc were used to collect Arc for study by QPCR, and these data showed that no genes important in POMC or NPY neuron physiology were changed in the pKO mouse. However, it is important to note that further work on the role of Lrh-1 in POMC neurons might uncover unknown functions that were not found over the course of this project. I safely conclude that the role of LRH-1 in POMC neurons may be subtle, complicated, but potentially important to the metabolic output of the animal under specific conditions.

References

Dampney, R. A. (2011). "Arcuate nucleus - a gateway for insulin's action on sympathetic activity." J Physiol **589**(Pt 9): 2109-2110.

Elmquist, J. K., C. F. Elias, et al. (1999). "From lesions to leptin: hypothalamic control of food intake and body weight." Neuron **22**(2): 221-232.

Parton, L. E., C. P. Ye, et al. (2007). "Glucose sensing by POMC neurons regulates glucose homeostasis and is impaired in obesity." Nature **449**(7159): 228-232.

Williams, K. W., L. O. Margatho, et al. (2010). "Segregation of acute leptin and insulin effects in distinct populations of arcuate proopiomelanocortin neurons." J Neurosci **30**(7): 2472-2479.

Zigman, J. M., J. E. Jones, et al. (2006). "Expression of ghrelin receptor mRNA in the rat and the mouse brain." J Comp Neurol **494**(3): 528-548.

CHAPTER SIX

Closing Remarks & Future Directions

6.1 Closing Remarks

The role of LRH-1 in metabolism has been a long and fruitful field of study and has allowed us to better understand the transcriptional mechanisms driving enterohepatic and reproductive processes. While decades of work have been spent on nuclear receptor biology in general, this present study underscores the importance of continuing the investigation of the function of nuclear receptors in less recognized areas of the body. The central nervous system is a relatively new organ of study in orphan nuclear receptor research. Many other orphan nuclear receptors besides LRH-1 can be found in the hypothalamus, brain stem, and other higher cortical regions, and their functions and significance are completely unknown. I hope that this project can encourage further research into exploring the roles of these nuclear receptors in the brain.

This study addresses two important questions. First, this study gives a definitive role for the orphan nuclear receptor LRH-1 in the arcuate nucleus of the hypothalamus. It was previously known that LRH-1 was expressed in the brain and was largely isolated to the arcuate nucleus. This study takes these observations further by demonstrating the importance of its selective expression in the arcuate nuclues of the brain. Second, this study details the process of how

kisspeptin neurons in the arcuate nucleus are able to influence FSH output by the pituitary during the follicular maturation phase of the female estrous cycle. It was previously known that kisspeptin neurons in the AVPV elicited the LH surge, but how kisspeptin neurons in either region of the brain worked to maintain FSH output was not known. These data here demonstrate the process of how kisspeptin neurons in the arcuate nucleus can maintain a set output of KISS1 peptide to stimulate the required level of FSH release from the pituitary. Importantly, these results complete the picture of how kisspeptin neurons in the two regions of the brain work in a temporally and spatially segregated manner to coordinate the process of estrous cyclicity and associated follicular maturation and ovulation.

6.2 Future Directions

An important observation during my time on this project was that DAX-1 was spatially segregated in a manner identical to LRH-1. DAX-1 was expressed in kisspeptin neurons of the arcuate nucleus, but not the AVPV. Similar to LRH-1, its expression levels in the arcuate nucleus increased during puberty and were modulated during the estrous cycle. DAX-1 is an orphan nuclear receptor that lacks a DNA binding domain. Instead, it binds to nuclear receptors and inhibits their ability to activate target gene transcription. It is known that DAX-1 can bind and inhibit both LRH-1 and ERα. Importantly, the inhibition of ERα by DAX-1 is dependent on the ligand binding status of ERα. In the absence of estradiol,

DAX-1 will not bind ERα. When ERα binds estradiol its AF-2 helix changes conformation to accept co-activator recruitment. DAX-1 binds to this activated conformation of the AF-2 helix, blocking co-activator access, and subsequently recruiting co-repressor complexes to shut down ERα activity.

With this in mind, it is easy to imagine a transcriptional system specific to kisspeptin neurons in the arcuate nucleus that involves DAX-1 transforming estradiol into an inhibitor of kisspeptin expression. In the AVPV, in the absence of DAX-1 expression, ERα would bind estradiol and induce kisspeptin expression. But in the arcuate, in the presence of DAX-1, the binding of estradiol by ERα would recruit DAX-1 and lead to repression of kisspeptin expression. Thus, while the segregated expression of LRH-1 is important for setting a basal level of kisspeptin expression during the follicular growth phase of the estrous cycle, the same segregated expression of DAX-1 could be required for selective repression of kisspeptin expression during the ovulatory phase.

The future directions of this project should focus on the role of DAX-1 in the arcuate nucleus. Considering that the mechanism allowing for estradiol's reciprocal roles during the estrous cycle has eluded the field of reproductive biology for decades, this could be a project with potentially incredible results. The first stage of the project should be the study of the loss of DAX-1 function in female mice. Construction of a kisspeptin specific DAX-1 knockout mouse is vital. There is no readily available DAX-1 floxed mouse so one should be

constructed. There is a total DAX-1 knockout mouse line available via Jackson Labs that can be reconstituted. It could be important to perform ovariectomy and estradiol replacement experiments in this total knockout mouse line to ascertain if there are any differences in kisspeptin's response to estrogen in the females. These results would be helpful, but it is important to remember that these mice suffer from a myriad of other adrenal and reproductive abnormalities. Therefore, construction of the kisspeptin specific DAX-1 mouse will be needed to specifically determine the requirement of DAX-1 for estradiol mediated kisspeptin repression in the arcuate nucleus.

The second stage of the project could focus on ChIP studies of Dax-1 binding to the kisspeptin promoter. *In vitro* and *in vivo* studies of DAX-1 and ERα interactions could also help complete a model of DAX-1 function in the arcuate nucleus. An interesting option would be the construction of a kisspeptin specific DAX-1 transgenic mouse, similar to the LRH-1 transgenic mouse used here. It was not discussed in this dissertation, but the Carol Elias lab has kisspeptin-cre driver mice that express cre specifically in the AVPV, or arcuate, but not both. It would be interesting to see the effects of inducing expression of DAX-1 in kisspeptin neurons in the AVPV. Would this lead to repression of kisspeptin expression in the AVPV and loss of the LH surge? That would be a striking finding that would definitively demonstrate the function of DAX-1 in mediating ERα activity in the hypothalamus.

A third stage of this project, a direction that was lacking in the work on LRH-1, could be the study of kisspeptin levels in human patients with DAX-1 mutations. Due to the developmental requirement of LRH-1, there have not been any humans found with LRH-1 mutations. DAX-1 was discovered because its mutation in human patients led to congenital adrenal and reproductive organ abnormalities. If hypothalamus tissue from female humans with mutations in DAX-1 could be obtained, it would be interesting to test kisspeptin mRNA or protein levels in these samples. One would expect that in the absence of functional DAX-1, kisspeptin levels may be higher in the arcuate due to the lack of ERα mediated repression. These experiments could offer a clinical correlate to the findings in mouse studies.

Hopefully, this work on LRH-1 has generated tools and materials that allow future scientists in this lab to study the function of other orphan nuclear receptors in the hypothalamus. The initial laser capture microdissection screen yielded an incredibly valuable map of the expression of all of orphan receptors in the different nuclei of the hypothalamus. Many of these are accessible for dissection and study, and continuing in these endeavors could uncover even greater pathways working to coordinate hypothalamic output with peripheral endocrine organ function.

CHAPTER SEVEN

Materials & Methods

7.1 Animal Housing and Mouse Generation

Kisspeptin specific LRH-1 knockout mice were generated using previously described KISS1-cre and *Lrh-1*$^{lox/lox}$ mouse lines (Lee, Schmidt et al. 2008; Cravo, Margatho et al. 2011). Tomato-red fluorescent reporter mice were created by crossing the KO mouse line with a previously generated TdT-Tomato mouse donated by Dr. Joel Elmquist. POMC specific *Lrh-1* knockout mice were generated using previously described POMC-cre and *Lrh-1*$^{lox/lox}$ mouse lines. NPY-GFP, POMC-GFP, and KISS1-GFP/KISS1-β-gal mice were previously generated donated by Dr. Joel Elmquist and Dr. Carol Elias labs. Transgenic mice were generated by the UT Southwestern Transgenic Core Facility using established protocols, and crossed with the KISS1-cre mouse line. After heterozygous crosses, all mice were maintained on a mixed C57Bl/6 x 129 genetic background. Mice were fed a standard chow diet containing 4% fat and absent of known estrogen receptor modulators (Harlan Teklad Global Diet; #2916). High fat "western diets" consistend of 60% kcals energy from fat (Harlan Teklad 60%kcal fat diet, high cholesterol diet). All experiments were performed on female mice at least 60 days of age, unless described otherwise. For tissue collection, the estrous cycle was followed for three days via vaginal flushing and

microscopic examination of vaginal epithelial cell morphology at 3pm daily (Thrasher, Clark et al. 1967; Nelson, Felicio et al. 1982). Mice verified to be in diestrous, or estrous, were killed via isoflurane overdose at 3pm. Arcuate nucleus, AVPV, and pituitary were dissected from the brain using an 11-blade scalpel and dissection scope on a dissection platform containing ice-cold RNAse-free phosphate buffered saline. Anatomical markers (i.e. location relative to 3rd ventricle, sella turcica, median eminence, optic chiasm, and internal capsule white matter tract) were used to accurately dissect each brain region. Collection of tissue via laser capture microdissection was done following standard procedures developed by the Dr. Elmquist lab. Tissues were snap frozen in liquid nitrogen and stored at -80°C. Both ovaries were collected. One was fixed in 10% RNAse-free formalin for 48 hours for histology, the other was snap frozen in liquid nitrogen and stored at -80°C. Plasma was collected using a 1ml Sub-Q 26g syringe via intracardiac puncture. Blood was allowed to coagulate at room temperature, cleared by centrifugation, and plasma collected and snap frozen in liquid nitrogen. Mouse FSH, LH, and estradiol levels were measured at the University of Virginia Ligand Core Lab using radioimmunoassay, multiplex, or ELISA, where applicable. Ovariectomy experiments were performed using a previously approved animal protocol (2009-0331). Briefly, age and weight matched WT and KO littermates were anesthetized with Avertin (2,2,2-tribromoethanol; SIGMA). On a heated surgical pad, a 1/2" midline dorsal

incision was used to access the intraperitoneal space on both sides of the animal. Ovaries were located and excised with minimal bleeding. Sham mice did not have ovaries removed. Proline sutures were used to close the animal. Animals recovered from anesthesia in a heated cage under supervision. Buprenorphine and saline were administered intraperitoneally three times over the next 48hr recovery period. After two weeks of recovery, mice were injected subcutaneously at 3pm with either vehicle (100% ethanol), or 6ug 17β-estradiol (Sigma) as previously described. 24hrs later mice were sac'd and arcuate nucleus collected. MRI body composition and metabolic cage analyses were performed at the UT Southwestern Metabolic Phenotyping Core facility in accordance with their standard protocols.

7.2 Estrous Cycle and Fertility Analysis

Six week old WT and KO littermates, two of each genotype, were placed together in fresh cages. Mice were allowed to equilibrate for 3 days before daily examination began. Estrous cycle was examined daily at 3pm using microscopic examination of vaginal epithelal morphology as described above. Mice were tracked for at least 8 weeks and % of time spent in each stage over the tracking period was calculated. This experiment was repeated across five different littermate groups, giving nearly identical results each time. Mice that never cycled were rejected from the study. Analysis of fertility was done by caging two WT or two KO 10 week old female mice in a cage with one male mouse. Mice

were allowed to breed and watched daily for litters. Litter number, and day of each litter was collected for at least four months per mating pair. These experiments were repeated three times with different littermates and stud males. The time between each litter was then calculated and averaged for each genotype.

7.3 In Situ Hybridization, Immunohistochemistry, and Histology

For ovarian histology, formalin fixed ovaries were washed in phosphate buffered saline and submitted to the UTSW Histology Core Facility. 25μm slices were collected every 100μm longitudinally through the ovary. Hematoxylin and eosin staining were performed. For Immunohistochemistry on female mouse brains, female mice were given a lethal i.p. injection of chloral hydrate (350mg/kg) and perfused transcardially with DEPC-treated 0.9% saline followed by RNAse-free neutral buffered 10% formalin. Brains were excised and fixed overnight in RNase-free 10% formalin, then cryoprotected with RNAse-free 20% sucrose overnight. 25μm coronal slices were collected using a sliding frozen microtome, and used for immunohistochemistry and in situ hybridization. Previously described techniques were used to visualize NPY, β-endorphin, or βGal using biotin conjugated antibodies and developed via peroxidase reaction with 3,3'-diaminobenzidine tetrahydrochloride (DAB; Sigma) (Scott, Lachey et al. 2009). Sections were mounted on gelatin-coated slides, dehydrated in increasing concentrations of ethanol, delipidated in xylenes, and coverslipped

with DPX mounting solution (Sigma). In situ hybridization was performed essentially as described elsewhere (Zigman, Jones et al. 2006). Briefly, a 500bp riboprobe specific to the 3'-UTR of LRH-1 was generated via *in vitro* transcription with ^{35}S-UTP. Free-floating brain sections were subjected to hybridization and mounted on superfrost + slides (Fisher). Slides were dipped in NTB photographic emulsion (Kodak, VWR), and stored in foil-wrapped slide boxes at 4°C for 3-4 weeks. Development was performed using Dektel developer (Kodak, VWR)

7.4 Fluorescent Assisted Cell Sorting

FACS collection and analysis of neurons was done as described in a previous publication (Cravo, Margatho et al. 2011). Female KISS1-GFP (n=6), NPY-hrGFP (n=3), POMC-hrGFP (n=4), or KISS1-cre^{+}-*Lrh-1*$^{-/-}$-tomato-red^{+} (n=4) were used for FACS. Female GFP- or tomato- mice were used in every experiment as negative controls. Briefly, Female mice were overdosed with isofluorane and decapitated. Brains were removed and arcuate nuclei were dissected and placed in ice-cold Hank's Balanced Salt Solution (HBSS, without calcium or magnesium (Gibco) in a 1.7ml microcentrifuge tube. Neurons were gently disassociated by replacing the solution with 500µl 5% Dispase in HBSS (v/v, Dispase: BD Biosciences) and incubating the tissue at 37°C for 10 minutes. Manual disassociation was performed at 5 minute intervals using a p200 pipette.

Dispase treatment was stopped by addition of 500µl FACS buffer (2.2ml 45% tissue-culture grade D+ glucose, 10µl 0.5M EDTA, 30mg fatty-acid free BSA, 10ml HBSS). Tissue was pelleted at 13,000rpm for 2 minutes. Supernatant was replaced with 500µl FACS buffer, and passed through a cell-strainer topped polypropylene tube (cell-strainer tops: BD falcon 5ml, pp polypropylene tubes: VWR). Samples were submitted to the UTSW Flow Cytometry Core Facility. Flow cytometry and cell collection using a MoFlow fluorescence activated cell sorter gating for GFP, or tomato-red was performed as described previously. RNA extraction was done using the PicoPure RNA Isolation kit (Arcturis). All steps in the MacroCap LCM instructions were followed, however, 100µl of extraction buffer and 100µl of 70% ethanol were used. RNA was extracted using 12µl of kit elution buffer. All 12µl of samples, as well as a standard curve of universal RNA (16ng to 0.5µg) was used in reverse transcription. Prior to qRT-PCR, cDNA was pre-amplified for genes of interest (*Kiss1, Npy, Pomc, Lrh-1*) using 2x TaqMan PreAmp Master Mix (Applied Biosciences) for 18 standard amplification cycles. Pre-amplified cDNA was diluted 20-fold in molecular grade water. qRT-PCR was performed using the procedures and primers described below.

7.5 qRT-PCR Analysis

All qRT-PCR protocols were carried out as previously described (Bookout, Cummins et al. 2006; Dutchak, Katafuchi et al. 2012). Primer Express

software (Applied Biosysems) and GenBank sequence data were used to design primers for qRT-PCR. Primers were selected to span exon junctions where applicable. RNA was extracted from tissues using RNA Stat-60 (Amsbio) and a tissue homogenizer. RNA was subjected to DNase-treatment (Roche) and cDNA synthesis (2µg) using the High Capacity cDNA Reverse Transcription kit (Applied Biosystems). qRT-PCR (10µl total) reactions contained 5µl of SYBR Green ER (Invitrogen), 25ng of cDNA, and 150nM forward and reverse primer. All reactions were performed in triplicate on an Applied Biosystems Prism 7900HT system. Relative mRNA levels were calculated against the internal control gene U36B4 using the comparative threshold cycle method. Primer sequences:

Lrh-1: forward: 5'-GAACTGTCCAAAACCAAAAAAGG-3'

reverse: 5'-CTTCCAGCTTCATCCCAAC-3'

Kiss1: forward: 5'-GGCAAAAGTGAAGCCTGGAT-3′

reverse: 5′-GATTCCTTTTCCCAGGCATT-3′

Npy: forward: 5'-CGCTCTGCGACACTACATCA - 3′

reverse: 5′-TCTCAGGGCTGGATCTCTTG-3′

Pomc: forward: 5′-TGCTTCAGACCTCCATAGATGTGT- 3′

reverse: 5′-GCGAGAGGTCGAGTTTGCA -3′

Cre: forward: 5'-TGTTGCCGCGCCATCTG-3'

reverse: 5'-TTGCTTCAAAAATCCCTTCCA-3'

StAR: forward: 5'-CGGAGCAGAGTGGTGTCATC-3'

reverse: 5'-TGAGTTTAGTCTTGGAGGGACTTC-3'

Cyp17a: forward: 5'-GGCTTTCCTGGTGCACAAT-3'

reverse: 5'-ACATACTGGTCAATCTCCTTTTGG-3'

Cyp19a1: forward: 5'-CCGAGCCTTGGAGAACAA-3'

reverse: 5'-AGGGCCCGTCAGAGCTT-3'

U36B4: forward: 5'-CGTCCTCGTTGGAGTGACA-3'

reverse: 5'-CGGTGCGTCAGGGATTG-3'

7.6 Chromatin Immunoprecipitation and Western Blot Analysis

Arcuate nuclei from female mice in diestrous (n=4) were collected at 3pm and immediately snap-frozen in liquid nitrogen. The Magna Chip-G Tissue kit (Millipore) was used to perform chromatin Immunoprecipitation for Lrh-1 on the kisspeptin promoter. The standard kit protocol was followed except extra care was taken to fully homogenize the tissue piece in tissue stabilization solution. A diagenode bioruptor bath sonicator was used on high at 10 cycles of 30 seconds on, 30 seconds off, with samples in TPX-hard walled tubes (Diagenode). Chromatin sonication was optimized and verified by agarose gel electrophoresis. A previously reported anti-human LRH-1 mouse monoclonal antibody (Perseus Proteomics PP-H2325-00, lot A2) was used in ChIP reactions. Normal mouse IgG

antibodies were used as negative IgG controls. qRT-PCR was used to measure fold enrichment over input. For all primers, on all plates, a standard input curve (10% input to .005% input; v/v) was used to normalize all samples for primer efficiency. Only primers with similar amplification efficiencies (as calculated by the slope of the log %input over avg. Ct value) were used. Normalized Ct data was expressed as fold enrichment over input. Fold enrichment of the negative control IgG fraction was checked in every experiment for every primer and never showed positive enrichment. These ChIP data were repeated on four separate cohorts of mice giving identical results every time. Primer sequences were designed using Primer Express:

-4400: forward: 5'-AAAGCTCCGCCTGCCTTA-3'

reverse: 5'-GGTGGCACATTCCTCCAAT-3'

-4100: forward: 5'-AAAGCTCCGCCTGCCTTA-3'

reverse: 5'-GGTGGCACATTCCTCCAAT-3'

-3700: forward: 5'-CCGGTCTCAGCTCACAGTACA-3'

reverse: 5'-AAGAAAGCCAGGTCAGATTGG-3'

-2300: forward: 5'-GGAGTTGGTTTTTCCCCTTCT-3'

reverse: 5'-CGCTTGACAATCTGAATTTAATCC-3'

-1000: forward: 5'-CCTAGGCTCCACCTGTTGTG-3'

reverse: 5'-CCCAACAAATGGCATTAAGTG-3'

+228: forward: 5'-GGCTGGTCTAGGCCCTTCT-3'

reverse: 5’-ACAGGACCCCCAACTCTAGCT-3’

+428: forward: 5’-CCATCCCAGCACTTGGAA-3’

reverse: 5’-TGTCCTGGACCAGGCTGAT-3’

+800: forward: 5’-CCCCCCAAGAGCATCATG-3’

reverse: 5’-CGAACAGCCAAGAAGAATTCA-3’

+1200: forward: 5’-GGCCACACTCACCTCCAA-3’

reverse: 5’ GCGGAGGATGGCTTTGA-3’

For western blot of Hek293 cells transiently transfected with CAG-*Z-Lrh-1* and CMV-Cre, Hek cells were collected in cell lysis buffer (20mM Tris HCl pH 7.5, 150mM NaCl, 1% Triton X-100, 5mM EDTA, 50mM NaF, 10mM β-glycerol phosphate, 1mM Na_3VO_4, 1mM PMSF and complete protease inhibitor cocktail). Protein concentration was determined by Bradford assay (Bio-Rad) and 30μg of protein was used in each SDS-PAGE gel. Blotting was performed on nitrocellulose membrane. Primary antibody incubation was performed in a solution of TBS containing 0.05% Tween and 5% BSA. Secondary antibody incubation was done in TBS-T containing 5% milk. Results were visualized using ECL western blotting substrates (Pierce). Primary antibodies included anti-human Lrh-1 antibody (PPMX) and anti- β-actin (SIGMA).

7.7 Cloning

Purified C57bl/6 mouse genomic DNA was used to clone ~4kb of the kisspeptin promoter using the Expand High Fidelity Taq PCR reagant (Roche). Primer ends were tailored to include restriction enzyme sites for site directed restriction digest. ATA- overhangs were added to each primer so PCR products could be TOPO cloned into the TOPO TA cloning vector for sequencing (Invitrogen). All cloned products were sequenced to verify the absence of mutations. Differing lengths of the promoter were sub-cloned into separate TOPO TA vectors. Restriction digest (NEB), gel purification (Qiagen), and subsequent ligation (NEB) into the pGL4-luc2 vector (Promega) was done using standard techniques. Antarctic phosphatase (NEB) was used where applicable. The resultant vectors included the full-length pKiss-luc, pKiss-3700-luc, and pKiss+228-luc. The QuikChange II XL Site Directed Mutagenesis kit (Agilent) was used to mutate the putative LRH-1 response element in the pKiss-luc vector. The entire promoter and Luc-locus of the vector was checked by sequencing to verify that only the two targeted base pairs were changed. The CAG-Z-MCS-IRES-EGFP transgenic vector was kindly donated by the Dr. Eric Olson lab and reported elsewhere. The mouse *Lrh-1* cDNA sequence was cloned into the multiple cloning site upstream of the IRES in the CAG-Z-MCS-IRES-EGFP vector. The completed vector was purified using an Endotoxin free plasmid prep kit (Qiagen). Restriction digest linearized the vector and removed bacterial expression elements. The linearized product was

purified for injection using low melt agarose gel, column purification, and phenol-clorophorm-isoamyl alcohol purification followed by isopropanol precipiation.

7.8 Cell Culture

Hek293 cells (ATCC) were passaged in phenol-red free DMEM (high glucose, no glutamine Invitrogen) with 10% delta-FBS (v/v; Gemini) without antibiotics using standard sterile cell culture technique. For luciferase assays, 80% confluent growing cells were split and resuspended in phenol-red free DMEM with 10% charcoal stripped FBS (v/v; Gemini) and plated into clear bottom, white sided 96-well luciferase plates at 50µl per well. The next day cells were transiently transfected using the previously described CaCl2 precipitation method (Makishima, Okamoto et al. 1999). All pKiss reporter vectors were transfected at 38ng DNA per well, and LRH-1 was transfected at 98ng DNA per well. 8ng of β-gal expression vector was used in all samples to normalize transfection efficiency, and empty pCDNA3.1 vector (Invitrogen) was used to equalize total DNA concentration transfected. Separate experiments using 98ng of reporter vector, and 38ng of LRH-1 were performed simultaneously and gave similar results. Luciferase and β-gal were developed 24 hours later using previously described techniques and read using a Wallac Victor^3 V 1420 spectrophotometer (Perkin Elmer). Luciferase values were normalized to β-gal values and expressed as fold induction over full-length pKiss reporter vector alone. All comparisons between

full-length pKIss and truncation/mutant vectors were performed on the same plate. These experiments were replicated at least 8 different times using different Hek293 passage number and reporter vector:LRH-1 ratios. For transient transfection assays of Cag-*Z-Lrh-1* and CMV-*Cre*, Hek293 cells in 24 well plates were transfected using the standard lipofectamine 2000 protocol (Invitrogen). 24 hours later cells were washed with phosphate buffered saline and EGFP expression visualized via inverted microscopy using 488nm excitation. LacZ was developed by fixing cells in formaldehyde for 5 minutes at room temperature (95ml 1xPBS, 5ml 37% formaldehyde, .2ml 25% glutaraldehyde; Sigma). They were then washed twice with 1xPBS, and stained in Stain Solution at 37□C until developed (80ml 1xPBS containing 50mM potassium ferricyanide, 50mM potassium ferrocyanide, .2ml 1mM $MgCl_2$, and 2ml X-gal in DMSO).

7.9 Statistical Analysis

Microsoft Excel 2007 was used for statistical analysis of data. Student's test of $p<.05$ was considered significant when comparing two groups

7.10 Image Generation and Analysis

Brain and ovary histology was analyzed using a Zeiss Axioplan microscope or Zeiss Axioscop2 microscope. Brightfield, darkfield, or epifluorescent viewing modes were used where appropriate. Images were collected with a CCD camera

and saved as high resolution TIFF files. For counting of double labeled cell populations, follicle number, follicle cysts, or corpus luteum, all images were numbered and counted blindly with respect to mouse genotype. For all cases, standard anatomical and histological criteria were used to identify specific structures or co-localizations.

References

Bookout, A. L., C. L. Cummins, et al. (2006). "High-throughput real-time quantitative reverse transcription PCR." Curr Protoc Mol Biol **Chapter 15**: Unit 15 18.

Cravo, R. M., L. O. Margatho, et al. (2011). "Characterization of Kiss1 neurons using transgenic mouse models." Neuroscience **173**: 37-56.

Dutchak, P. A., T. Katafuchi, et al. (2012). "Fibroblast Growth Factor-21 Regulates PPARgamma Activity and the Antidiabetic Actions of Thiazolidinediones." Cell **148**(3): 556-567.

Lee, Y. K., D. R. Schmidt, et al. (2008). "Liver receptor homolog-1 regulates bile acid homeostasis but is not essential for feedback regulation of bile acid synthesis." Mol Endocrinol **22**(6): 1345-1356.

Makishima, M., A. Y. Okamoto, et al. (1999). "Identification of a nuclear receptor for bile acids." Science **284**(5418): 1362-1365.

Nelson, J. F., L. S. Felicio, et al. (1982). "A longitudinal study of estrous cyclicity in aging C57BL/6J mice: I. Cycle frequency, length and vaginal cytology." Biol Reprod **27**(2): 327-339.

Scott, M. M., J. L. Lachey, et al. (2009). "Leptin targets in the mouse brain." J Comp Neurol **514**(5): 518-532.

Thrasher, J. D., F. I. Clark, et al. (1967). "Changes in the vaginal epithelial cell cyle in relation to events of the estrous cycle." Exp Cell Res **45**(1): 232-236.

Zigman, J. M., J. E. Jones, et al. (2006). "Expression of ghrelin receptor mRNA in the rat and the mouse brain." J Comp Neurol **494**(3): 528-548.